

# Performance of the 4-m International Liquid Mirror Telescope tested in two fields at high and low ecliptic and galactic latitudes

Sara Filali<sup>1,\*</sup>, Kumar Pranshu<sup>2,3</sup>, Jean Surdej<sup>1,2</sup>, Paul Hickson<sup>4,5</sup>, Kuntal Misra<sup>2</sup>, Bhavya Ailawadhi<sup>2,6</sup>, Talat Akhunov<sup>7,8</sup>, Monalisa Dubey<sup>2,9</sup>, Naveen Dukiya<sup>2,9</sup>, Brajesh Kumar<sup>10</sup>, Priyanshi Kumari<sup>2</sup>, Vibhore Negi<sup>11</sup>, and Anna Pospieszalska-Surdej<sup>1</sup>

<sup>1</sup>Institute of Astrophysics and Geophysics, Liège University, Allée du 6 août 19c, 4000 Liège, Belgium.

<sup>2</sup>Aryabhata Research Institute of Observational Sciences, Manora Peak, Nainital, Uttarakhand, 263001, India.

<sup>3</sup>University of Calcutta, 87/1 College Street, Kolkata, 700073, India.

<sup>4</sup>Department of Physics and Astronomy, The University of British Columbia, 6224 Agricultural Road, Vancouver, BC, V6T 1Z1, Canada.

<sup>5</sup>Outer Space Institute, The University of British Columbia, 325-6224 Agricultural Rd., Vancouver, BC, V6T 1Z1.

<sup>6</sup>Deen Dayal Upadhyay Gorakhpur University, Civil Lines, Gorakhpur, Uttar Pradesh, 273009, India.

<sup>7</sup>National University of Uzbekistan, Department of Astronomy and Astrophysics, 100174 Tashkent, Uzbekistan.

<sup>8</sup>Ulugh Beg Astronomical Institute of the Uzbek Academy of Sciences, Astronomicheskaya 33, 100052 Tashkent, Uzbekistan.

<sup>9</sup>Mahatma Jyotiba Phule Rohilkhand University, Pilibhit Bypass Road, Bareilly, Uttar Pradesh, 243006, India.

<sup>10</sup>South-Western Institute for Astronomy Research, Yunnan University, Kunming 650500, Yunnan, P. R. China.

<sup>11</sup>Inter University Center for Astronomy and Astrophysics, Post Bag 4, Ganeshkhind, Pune 411007, India.

\*Corresponding author. E-mail: sfilali@uliege.be

**Abstract.** The 4-m International Liquid Mirror Telescope (ILMT) offers a unique opportunity to detect transients in a narrow strip of sky. We explore ILMT's potential to detect astrometric and photometric transients at various ecliptic and galactic latitudes. We inspected CCD frames observed at both low and high ecliptic and galactic latitudes during the commissioning phase and the November 2023 - May 2024 observation cycle, respectively. We analysed these images using both visual inspection and the ILMT's transient detection and candidate classification pipeline. In the low ecliptic and galactic latitude field, we detected more than 500 transient candidates. We cross-matched these with the Minor Planet Checker (MPC) database, identifying 504 catalogued asteroids, all with predicted V-magnitudes brighter than 24 mag, representing a total of 152 distinct asteroids. We performed the same steps on the high ecliptic and galactic latitude field, detecting 30 MPC-catalogued asteroids, and one newly discovered photometric transient, named AT 2024fxn. We present the positions, trajectories, and magnitudes of the detected asteroids observed in the SDSS  $g'$ ,  $r'$ , and  $i'$  spectral bands and compare results from both fields. We explore the lightcurve of AT 2024fxn, which shows partial compatibility with a supernova (SN) hypothesis, while the data invites further insights.

**Keywords.** Telescopes, Liquid Mirror Telescopes—Minor planets, asteroids—Astrometry—Methods: data analysis—Techniques: image processing—Techniques: photometric

## 1. Introduction

The International Liquid Mirror Telescope (ILMT) is a telescope dedicated to photometric and astrometric survey, installed at the Devasthal observatory in the foothills of the Himalayas at 2378 m altitude and (29°21'41.4", 79°41'07.08") latitude and longitude. The telescope is permanently oriented toward the zenith, enabling it to continuously scan the same strip of the sky centred around the declination corresponding to the latitude of the site. As a result, its cadence

is approximately one day under optimal conditions, except when affected by meteorological conditions. It is equipped with a 4096×4096 pixel CCD camera that operates in the Time Delay Integration (TDI) mode (Gibson & Hickson, 1992; Surdej *et al.*, 2024; Surdej *et al.*, 2025), with an integration time  $t_{int} = 102.35$  s. The CCD camera has a field of view of 22.3' x 22.3' and the signal integration operates along the right ascension ( $\alpha$ ). The acquisition time of a single long CCD/TDI frame is approximately 17-min, corresponding to ten-fold the integration time. Each portion of the strip ob-

served over this timeframe, excluding the first ramping 22.3' x 22.3' image, constitutes an individual frame of the ILMT, having a width of 22.3' along the declination (Dec) and a length of 200.7' along  $\alpha$ . The high cadence of the telescope, its large diameter and small focal ratio ( $f/D \approx 2.4$ ), make it a unique tool to detect minor planets (for more details on the ILMT, refer to Surdej *et al.* 2018, 2024).

The ILMT has completed four observing cycles at the time of writing this paper: April–May and October–November 2022, March–June 2023, November 2023–May 2024, and October 2024–June 2025. At the beginning of the commissioning phase in October–November 2022, we recorded 20 contiguous CCD frames with the  $g'$ ,  $r'$ , and  $i'$  SDSS spectral filters. From these, we selected a 1.24 square-degree field corresponding to a single CCD footprint, observed repeatedly over nine nights and in three different filters. The field starts at  $\alpha_{2000} = 4\text{h } 50\text{m}$ , corresponding to low ecliptic and galactic latitudes ( $6^\circ \lesssim \beta \lesssim 7^\circ$ ,  $-10^\circ \lesssim b \lesssim -7^\circ$ ). We refer to this region as Field 0450 to reflect its right ascension.

We subsequently analysed images acquired during February–May 2024, concentrating on a 6.22 square-degree field starting at  $\alpha_{2000} = 13\text{h } 17\text{m}$  and corresponding to high ecliptic and galactic latitudes ( $35^\circ \lesssim \beta \lesssim 43^\circ$ ,  $66^\circ \lesssim b \lesssim 82^\circ$ ), which we refer to as Field 1317. In contrast to Field 0450 described earlier, this larger angular area was selected to ensure a sufficient coverage of transients, thereby enabling a robust statistical analysis. Our goal was to assess the potential of the ILMT observations at different ecliptic and galactic latitudes.

The paper is structured as follows. In Section 2., we present the methodology, results, and analysis of asteroid detections in both fields. In Section 3., we present the methodology, results and analysis of the detected photometric transient AT 2024fxn. In Section 4., we draw conclusions regarding the overall detections. In Appendix C, we provide the detected asteroid tables. Details on these tables can be found in Appendix A and Appendix E. Appendix B describes the photometric parameters used for the asteroid measurements, with the reported uncertainties limited to zero-point variations, while the full photometric uncertainty budget is described and discussed in Section 2.2.

## 2. Asteroids

### 2.1 Detection methodology

In Field 0450, we examined 9 CCD frames visually as well as with the PyLMT automated transient detection and candidate classification pipeline (Pranshu

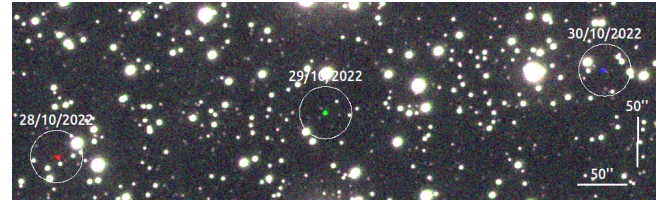


**Figure 1:** Visual detection through RGB stacking. Red, green, and blue represent detections of the asteroid Melanthios on the nights of 28, 29, and 30th of October 2022, respectively, all obtained with the same  $i'$ -SDSS filter. North is up, and East is to the left. The RGB method highlights temporal changes by assigning a distinct color component to each nighttime frame.

*et al.*, 2025). For the visual inspection, we employed the DS9 software (Joye & Mandel, 2003), applying the blinking method to some frames, and the RGB stacking method to others (cf. Pospieszalska-Surdej *et al.* 2024). In the RGB stacking method, we aligned three frames captured on different nights, assigning each frame to one of the RGB color channels. In the resulting image, most sources appear white, while astrometric transients stand out in different colors depending on the night of observation. Figure 1 shows an example of visual detection through RGB stacking in Field 0450. The PyLMT pipeline combines a subtraction technique module, a transient search and candidate classification module utilising a convolutional neural network (CNN), and a candidate cross-checking module (Pranshu *et al.*, 2025). Applying both the visual and the PyLMT methods independently, we pinpointed several hundred transient candidates in total, with the PyLMT alone detecting 496 candidates. We cross-matched both methods and incorporated the exclusively visual detections in the PyLMT software to refine its detection parameters. Subsequently, we compared the combined detections from both approaches against the Minor Planet Center (MPC) database, and identified 504 detections of known asteroids within this field, corresponding to 152 distinct asteroids. These objects display predicted  $V$ -magnitudes ranging between 16 and 24 mag. Although our limiting magnitude is estimated at  $V \approx 22$ , we retained  $V = 24$  mag as the threshold to include a representative set of faint MPC-predicted asteroids for completeness assessment, while keeping the sample within a manageable range. This choice also means that the reported detection percentages are conservative; restricting the MPC search to  $V \leq 22$  (Surdej *et al.*, 2025) would have increased these rates. Detection rates are: 130 detections out of 271 MPC predictions in the  $g'$  band ( $\sim 48\%$  detection rate), 210 out of 286 in the  $r'$  band ( $\sim 73.4\%$ ), and 164 out of 257 ( $\sim 63.8\%$ ) in the  $i'$  band. Details of these detections are

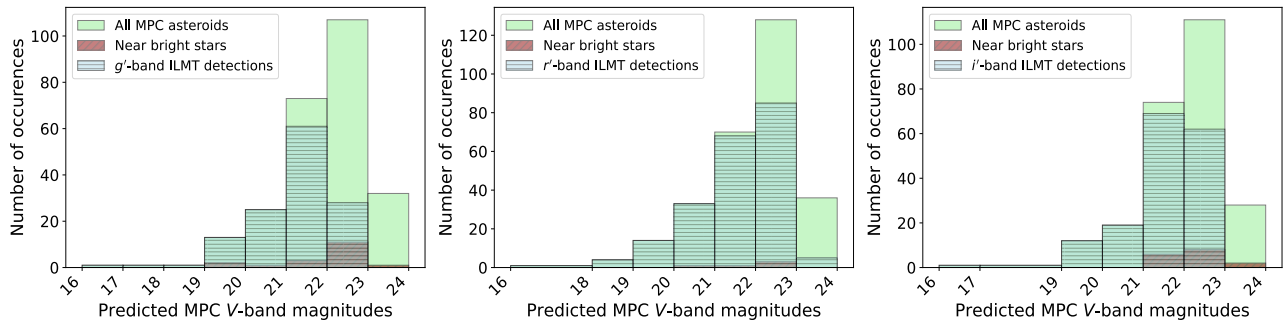


**Figure 2:** Distribution of the MPC-predicted  $V$ -band magnitudes of asteroids detected in Field 0450 through the  $g'$ ,  $r'$ , and  $i'$  SDSS spectral filters.

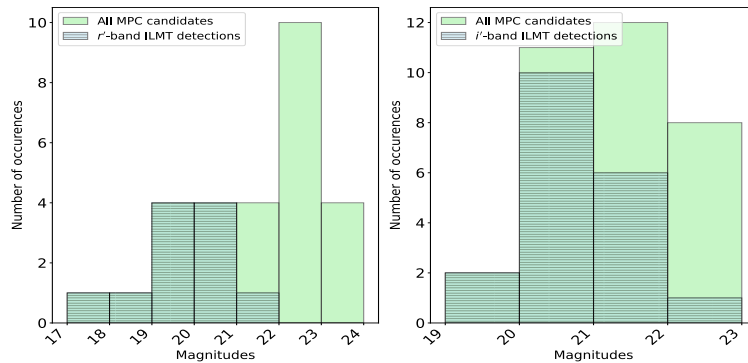


**Figure 3:** Distribution of the MPC-predicted  $V$ -band magnitudes of asteroids detected in Field 1317 through the  $r'$  and  $i'$  SDSS spectral filters.

presented in Appendix C, and their  $V$ -magnitude distributions are presented in Figure 2.

In Field 1317, we analysed 19 CCD frames observed with the ILMT in the  $r'$  and  $i'$  bands. The MPC predicted 61 asteroids, and we applied the now finetuned PyLMT pipeline for independent detection and classification, where image subtraction has been executed using frames from the same cycle as references. We performed a subsequent visual examination solely for confirmation. In total, 30 asteroids were detected by the PyLMT, out of which 22 are distinct ones. Detection rates are 11 out of 28 MPC predictions ( $\sim 39.3\%$ ) in the  $r'$  band, and 19 out of 33 ( $\sim 57.6\%$ ) in the  $i'$  band. Differences in detectability with Field 0450 are explained by variations in the sky quality during observations. Additionally, the presence of more fainter asteroids in Field 1317, particularly in the 23–24 magnitude range, may have contributed to this effect. The  $V$ -magnitude distributions of these detections are presented in Figure 3. Defining the limiting recall magnitude as the magnitude at which half the asteroids are detected, Figure 2 shows that the ILMT limiting recall  $V$ -magnitudes using the PyLMT pipeline in Field 0450 are 21.5, 22.0, and 22.0 in the  $g'$ ,  $r'$ , and  $i'$  bands, respectively (conservative estimates). For Field 1317,

Figure 3 indicates that the limiting recall magnitude is 21 in both the  $r'$  and  $i'$  bands, also based on conservative estimates.

## 2.2 Magnitude and position measurements

The typical point spread function (PSF) in our images has a mean full width at half maximum (FWHM) of approximately 1.5 arcsec and is close to circular across all filters, with median ellipticities  $e \leq 0.04$  in the  $r'$  and  $i'$  bands and  $e \approx 0.12$  in the  $g'$  band. The slightly higher ellipticity measured in the  $g'$  band is attributed to the less optimal corrections of the optical corrector (optimised in the spectral range  $\lambda \approx 5500 - 7500\text{\AA}$ ) and the lower signal-to-noise ratio (S/N) of the  $g'$  exposures, rather than to systematic tracking-induced elongation, indicating that the exposures themselves do not introduce significant elongation. This is a result of the 5-lens asymmetric optical corrector (Hickson & Richardson, 1998) installed at the prime focus of the ILMT, which compensates for the nonlinear motion of stars in the images and largely eliminates TDI distortions.

After examining the apparent sky-plane rates of motion provided by MPCchecker for asteroids in Fields 0450 and 1317, we found that the median asteroid motions in both fields are below 35 arcsec/hr. For the ex-

posure time of 102.35 s, this corresponds to a displacement of approximately 1 arcsec, which is smaller than the measured stellar PSF FWHM. Therefore, any elongation due to asteroid motion is small relative to the PSF, and asteroids can be treated as effectively point-like for the purposes of aperture photometry. Thus, there is no need to consider a possible elongation of the PSF for the detected asteroids, and circular photometric apertures were used throughout the analysis. For the small number of sources exhibiting visually elongated or poorly defined centroid profiles (due to low S/N or unusually high motions), the corresponding photometric measurements were flagged as uncertain and treated accordingly in the subsequent analysis. We employed two distinct methods for estimating magnitude and position, depending on the location of the target asteroid within the CCD frame:

- *The statistical method:* This method involves a statistical approach. The photometric zero point is estimated for each long CCD frame using Gaia reference stars present in it. The FWHM of the PSF is also estimated for each frame, rather than for individual objects (Hickson, 2019). The positions are estimated by fitting a centroid profile to each PSF, and aperture photometry is then applied with a radius of  $2 \times FWHM$ . If the studied asteroid is located in a crowded region or in a region with high background gradient, we measured its magnitude using the *individualised* method.
- *The individualised method:* Aperture photometry is applied on the given asteroid using the imexam library (Sosey, 2017), which is affiliated to the Astropy project (Price-Whelan *et al.*, 2018). The zero point for each asteroid is estimated by utilising neighbouring reference stars, with their number usually ranging between 3 and 7, and occasionally equal to 2. These stars are selected to minimise the root mean square (RMS) deviations of the magnitude zero points and the angular distances to the target asteroid. The asteroid's position is obtained by fitting a Gaussian profile to its recorded image.

Figures 4 and 5 display the paths of asteroids as determined from position measurements within their respective fields. Furthermore, we plotted the  $g'$ ,  $r'$ , and  $i'$  measured magnitudes versus the MPC-predicted  $V$ -magnitudes in Field 0450 and applied linear regression, as shown in Figure 6. The obtained relations are:

$$g' = (0.94 \pm 0.01) V + (1.46 \pm 0.11) \quad (1)$$

$$r' = (0.98 \pm 0.01) V + (0.31 \pm 0.08) \quad (2)$$

$$i' = (1.00 \pm 0.01) V - (0.38 \pm 0.07) \quad (3)$$

where  $g'$ ,  $r'$ , and  $i'$  are the SDSS magnitudes derived from the ILMT observations, and  $V$  is the apparent magnitude predicted by the MPC based on the object's orbital elements and absolute magnitude ( $H$ ). The quality of each fit is quantified by the chi-squared statistic: for the  $g'$  band,  $\chi^2 = 702.21$  with 118 degrees of freedom (DOF) and reduced  $\chi^2 \approx 6.0$ ; for the  $r'$  band,  $\chi^2 = 1293.58$  with 182 DOF (reduced  $\chi^2 \approx 7.1$ ); and for the  $i'$  band,  $\chi^2 = 1034.02$  with 139 DOF (reduced  $\chi^2 \approx 7.4$ ). Uncertainties on the measured magnitudes include zero-point deviations estimated from neighboring stars, as well as statistical uncertainties including readout noise, Poisson noise, and background noise. Points that deviate significantly from the fitting line correspond to uncertain magnitudes, typically caused by zero point variations or poor PSF fitting. These cases are noted in Appendix E and illustrated in Appendix D (Figure 12), which shows representative cutouts of flagged objects. This deviation could also be explained by rotational photometric variability, in which the asteroid's rotation changes the fraction of sunlight reflected toward the observer, which is not taken into account in the MPC magnitude predictions. When the rotational phase at the time of our observation differs from that of the MPC reference data, this produces additional point-to-point scatter.

The slopes in Equations 1, 2, and 3 are close to unity, indicating overall consistency between our photometry and the MPC predictions. However, the reduced  $\chi^2$  values are significantly larger than unity in all bands, indicating residual scatter beyond the quoted uncertainties.

To account for this, an additional uncertainty floor was added in quadrature to the individual magnitude uncertainties. The value of this additional term was determined by requiring the reduced  $\chi^2$  of the fit to be close to unity, thus accounting for underestimated errors and unmodeled systematics, and was then applied uniformly to all data points. The resulting uncertainty floors are 0.36, 0.32, and 0.35 mag in the  $g'$ ,  $r'$ , and  $i'$  bands, respectively. The resulting color-transformation relations are:

$$g' = (0.92 \pm 0.04) V + (2.05 \pm 0.73) \quad (4)$$

$$r' = (0.97 \pm 0.02) V + (0.54 \pm 0.49) \quad (5)$$

$$i' = (1.00 \pm 0.03) V - (0.27 \pm 0.66) \quad (6)$$

The updated fits suggest that the scatter is real and likely reflects systematic effects, such as inaccuracies in the MPC  $H$  and  $G$  parameters (as noted by Juric *et al.* 2002; Pravec *et al.* 2012; Vereš *et al.* 2015), and color-dependent offsets due to the lack of full transformation corrections. The fitted intercepts in Equations 4, 5, and 6 reveal non-negligible photometric offsets:

when both the original and adjusted intercepts are considered, MPC magnitudes tend to be brighter than our SDSS-based estimates by approximately 1.5–2.1 mag in  $g'$ , about 0.3–0.5 mag in  $r'$ , and about 0.3–0.4 mag fainter in  $i'$ . While part of these offsets may result from the simplified V-band transformation from SDSS filters, which does not fully account for filter differences and asteroid color variations, they also reflect known limitations in the current MPC H and G estimates, as well as possible biases introduced by rotational photometric variability.

### 2.3 Detection results

In total, we have made 504 detections of 152 distinct catalogued asteroids in Field 0450, and 30 detections of 22 distinct catalogued asteroids in Field 1317, with predicted  $V$ -magnitudes ranging from 16.4 to 23.6 and from 17.1 to 21.6, respectively. Table 1 lists the number of asteroids having been observed 1, 2, 3 or more times on different nights. The small number of asteroids observed during several nights is due to their higher average angular speed. The list of the overall detections is provided in Appendix C. Many of these asteroids exhibit a complex detection status, particularly in Field 0450: some detections are too faint and approach the detection limit, while others are situated near bright stars that either entirely or partially occult their recorded images. These distinct cases are classified under ‘Class’ in the tables of Appendix C, with detailed explanations for the different classes adopted in Appendix A. Zoomed images of asteroids from the different classes are shown in Appendix D (Figure 13). Positions obtained with both methods have an accuracy better than 0.4 arcsec.

### 2.4 Angular distance calculation

For each detection, we calculated the angular distance  $d$  between the MPC-predicted and the ILMT-observed positions:

$$d = \arccos(\sin(Dec_{obs}) \sin(Dec_{MPC}) + \cos(Dec_{obs}) \cos(Dec_{MPC}) \cos(\alpha_{MPC} - \alpha_{obs})) \quad (7)$$

where  $\alpha_{obs}$ ,  $\alpha_{MPC}$ ,  $Dec_{obs}$ ,  $Dec_{MPC}$  are the observed and the MPC-predicted right ascensions, and the observed and MPC-predicted declinations of the asteroid, respectively.

### 2.5 Astrometric analysis

As far as the ILMT observations are concerned, we have determined the UTC at which an asteroid was

observed from its right ascension, which exactly corresponds to the local sidereal time when the asteroid crossed the central row of the CCD. This UTC is accurate to within several seconds at most.

When using the Minor Planet Checker (MPCChecker) to find the predicted position of the same asteroid, we can only specify the observation date with a precision of 0.01 day<sup>1</sup>, i.e., 14.4 minutes. For instance, if the ILMT UTC is 13h 08m 02s on 14 August 2024, the date to be entered in the MPC Checker should be: 2024 08 14.55. The MPCChecker then provides the positions in RA and Dec of the closest asteroids to our measured RA and Dec. The angular separations are calculated using the previously given equation, based on these MPC positions and the ILMT observed positions.

However, the indicated MPCChecker epoch corresponds to an MPC UTC of 13h 12m 00s. During the time difference between the ILMT UTC and the quoted MPC UTC,  $\Delta t = 3 \text{ min } 58 \text{ s}$ , the asteroid moved by an angle equal to  $v \times \Delta t$ , where  $v$  is the asteroid’s angular velocity. The equatorial components of these angular velocities are also provided by the MPCChecker. After correction for these motions, the offsets between the observed ILMT positions and the corrected MPC ones give rise to the corrected histograms illustrated in Figure 7 for the Field 0450 and Field 1317.

The measured angular separations between MPC-predicted and ILMT-observed positions of detected asteroids remain limited, ranging from 0'' to 6.9'' in Field 0450 and from 0'' to 6.5'' in Field 1317. The complete range of angular separations is mentioned in the tables of Appendix C.

Numerically, we expect typical differences between MPC-predicted and our observed positions to mostly range between 0'' and 3.1'', with possible values reaching up to 5.3'' in Field 0450. In Field 1317, differences generally range between 0'' and 6.3''. These expectations justify our choice of separation thresholds for secure identification.

For each detection, we considered the identification secure if the angular separation between the observed and MPC-predicted positions is less than 3''. Figure 7 shows the histogram of residual angular separations in Fields 0450 and 1317. When the separation exceeds this threshold, we performed a detailed analysis of the equatorial separation components  $\Delta RA \cdot \cos(Dec)$ ,  $\Delta Dec$  in relation to the instantaneous velocity components provided by the MPC at the observation time. Specifically, for each detection, we computed the expected positional shift in each coordinate with:

<sup>1</sup><https://www.minorplanetcenter.net/cgi-bin/checkmp.cgi>

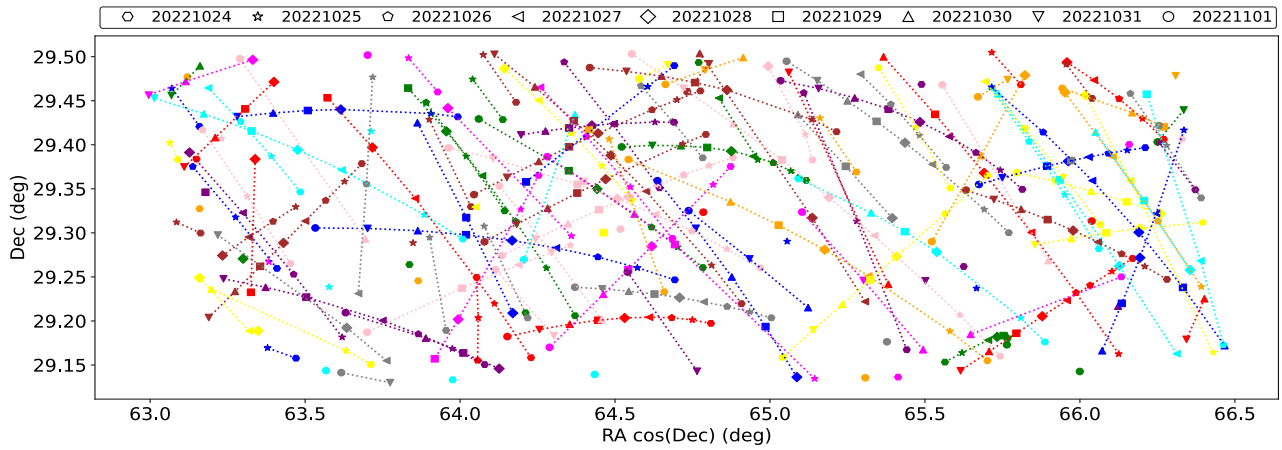


**Figure 4:** Positions and paths of the 504 asteroids detected with the ILMT in Field 0450 during the 24/10/2022 - 01/11/2022 nights. A unique color was assigned to each asteroid by cycling through a fixed color palette. Although some colors may correspond to more than one object, each asteroid is consistently represented by a single color and path across the figure. Three of the detected asteroids are confirmed to exhibit prograde motion, while 108 are confirmed to exhibit retrograde motion.

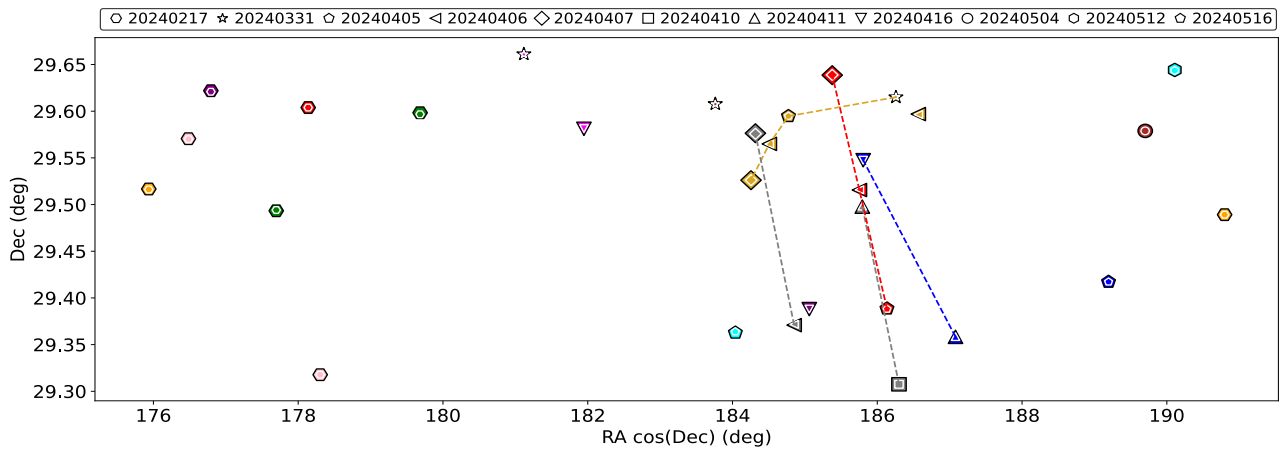


**Figure 5:** Positions and paths of the 30 asteroids detected with the ILMT in Field 1317 during the 14/02/2024 to 16/05/2024 nights. Observed and MPC-predicted positions share the same color per asteroid, though colors may repeat across different asteroids. Observed positions have larger markers with black edges; predicted positions have smaller markers with white edges, so predicted points appear inside observed ones—illustrating the close angular separations. Observed paths are shown with dashed lines. None exhibits prograde motion, and five are confirmed to exhibit retrograde motion. As expected, due to the higher ecliptic latitude of Field 1317, far fewer asteroids are detected compared to the Field 0450.

**Table 1:** Frequency of observation of the asteroids with the ILMT during its nine commissioning nights from October 24 to November 01, 2022, and during the nights between February 14 and May 16, 2024. The first column indicates the number of nights they were observed. The second and third columns indicate the number of asteroids.

Nights	Asteroids in Field 0450	Asteroids in Field 1317
1	41	17
2	33	3
3	27	1
4	14	1
5	7	0
6	7	0
7	8	0
8	8	0
9	7	0

$$\Delta RA_{\text{pred}} \cdot \cos(\text{Dec}) = v_{\text{RA}} \cdot \Delta t, \tag{8}$$

$$\Delta \text{Dec}_{\text{pred}} = v_{\text{Dec}} \cdot \Delta t. \tag{9}$$

where  $\Delta RA$  and  $\Delta Dec$  are the angular differences between the observed and MPC-predicted positions in equatorial coordinates, the  $\cos(\text{Dec})$  factor is computed using the MPC-predicted declination,  $\Delta t$  is the time offset between the MPC-reported epoch (rounded to 0.01 days) and the precise time of our observation, and  $v_{\text{RA}}$  and  $v_{\text{Dec}}$  are the equatorial components of angular velocity provided by the MPC, with  $v_{\text{RA}}$  already including the  $\cos(\text{Dec})$  factor. If the difference between observed and theoretical displacements is less than  $2''$  in both coordinates, the identification was confirmed; otherwise, it was classified as uncertain and flagged accordingly in the detection tables. Applying this criterion, only 4 out of 504 detections in Field 0450 were flagged as uncertain, whereas all detections in Field 1317 were confirmed. The correlation between the expected and measured angular separations is strong in both fields, with Pearson coefficients of 0.82 and 0.79 for Fields 0450 and 1317, respectively (see Figure 8).

As shown in this section, the MPC-based cross-checking introduces a time uncertainty that requires the statistical framework presented in this section. This could in principle be avoided by identifying candidate asteroids via MPChecker and retrieving their higher-precision ephemerides directly from NASA’s JPL Horizons (Giorgini *et al.*, 1996). However, the precision achieved is already sufficient for the scientific objectives of this study. We therefore leave the integration of JPL Horizons ephemerides as a possible refinement for future work, where it could both simplify the cross-matching procedure and enhance its astrometric precision.

### 2.6 Photometric analysis

We have presented in Figure 9 the SDSS magnitude histograms of asteroids detected in Field 0450 under very favorable seeing and sky transparency conditions. As shown in that figure, detections reach 22.9, 22.9, and 22.4 in the  $g'$ ,  $r'$ , and  $i'$  bands, respectively. This finding is very encouraging.

## 3. Photometric transient: AT 2024fxn

### 3.1 Methodology

While running the PyLMT pipeline for Field 1317, we detected several transients that the pipeline classified as belonging to extended hosts. From these, we aimed to select one transient with repeated observations and a noticeable brightness change. We recognised a candidate at the position  $\alpha_{2000} = 14:13:49.60$ ,  $\delta_{2000} = +29:23:32.0$ .

This transient has been observed in the  $r'$  and  $i'$  bands during 9 different nights with a seeing around  $1.8''$ , and a first rise in flux observed on April 5th, 2024. The PyLMT classified it as belonging to an extended host with a CNN confidence score of (0.95173323, 0.9997887), representing classification and detection scores, respectively (Pranshu *et al.*, 2025); thus, a possible supernova. We sent an alert to the Transient Name Server (TNS)<sup>2</sup> and the transient has been designated AT 2024fxn (Pranshu *et al.*, 2024). In the following hours and days, AT 2024fxn has been reported by ATLAS (Tonry *et al.*, 2018), the Zwicky Transient Facility (ZTF, Bellm *et al.*, 2018) and Pan-STARRS (Magnier *et al.*, 2020), with an excellent agreement in position.

<sup>2</sup><https://www.wis-tns.org/object/2024fxn/discovery-cert>

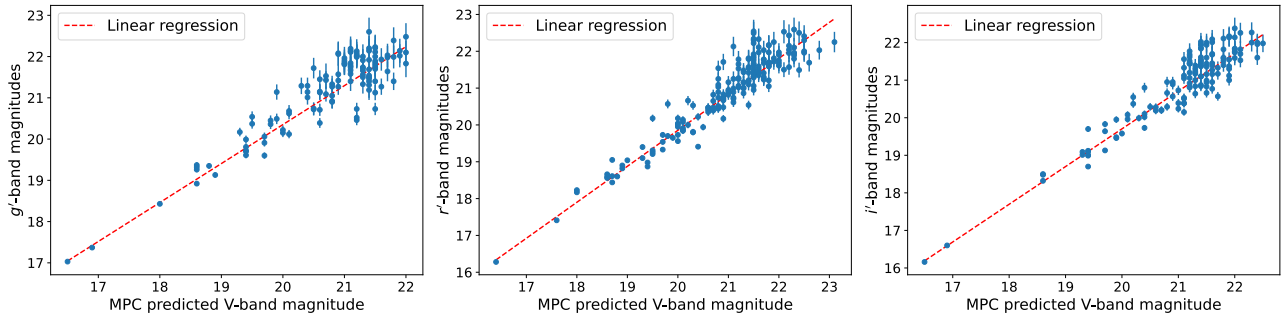


**Figure 6:** Measured SDSS-band magnitudes versus MPC-predicted V-band magnitudes for the detected asteroids in Field 0450.

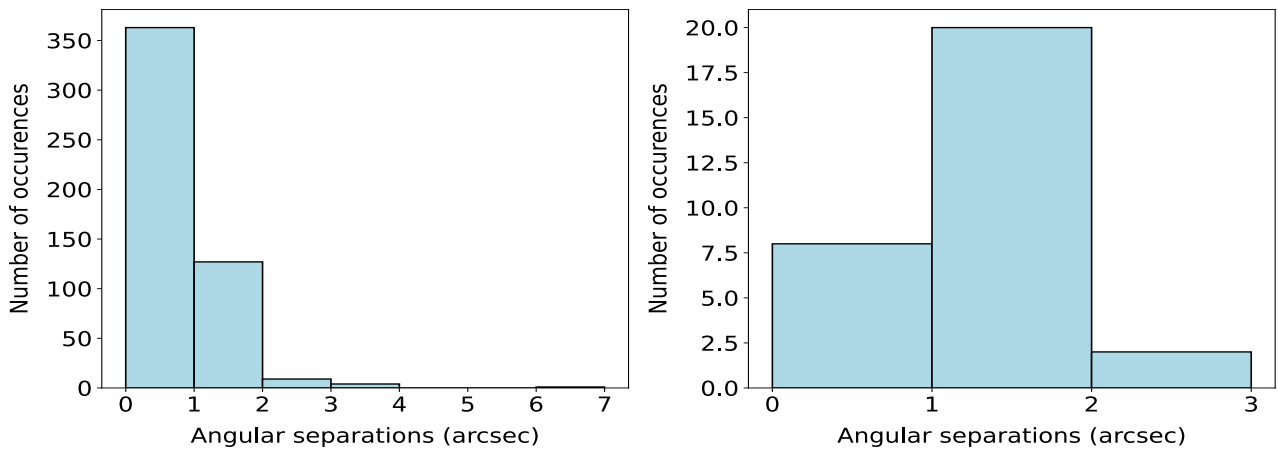


**Figure 7:** Histogram of residual angular separations for asteroids detected in Field 0450 (left) and Field 1317 (right).

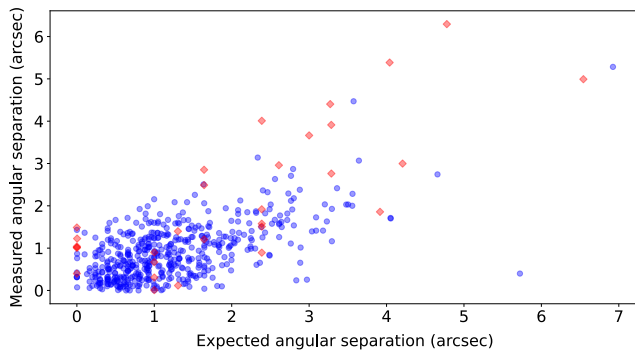


**Figure 8:** Scatter plot of expected versus measured angular separations between ILMT-observed and MPC-predicted positions of the detected asteroids. Blue markers represent data from Field 0450 and red markers represent data from Field 1317.

We then identified the corresponding science frames containing AT 2024fxn. The  $g'$ -band provides no usable constraints, as only one underexposed frame was obtained. While several  $i'$ -band frames are available, their low signal-to-noise due to poor observing conditions results in uncertainties too large for meaningful photometry. Consequently, the photometric analysis is restricted to the  $r'$ -band. Although the  $i'$ -band data are not suitable for photometric analysis, image subtraction was nevertheless performed to assess the presence and morphology of the transient; we therefore reconducted a subtraction based on the same reference image per filter, using our custom built ILMTDiff image subtraction software (Pranshu *et al.*, 2025) over a square cutout of  $2048 \times 2048$  pixels. For the subtraction to be of ideal quality, reference images should present a better seeing than science images, and a low background level (Pranshu *et al.*, 2025). Therefore, we used specific reference images from 15-02-2024 for the  $r'$ -band and from 08-02-2024 for the  $i'$ -band. Figure 10 illustrates the results of these subtractions.

We proceeded with the construction of the lightcurve of AT 2024fxn by combining ILMT data with those from the ZTF, noting that the ZTF  $r$ -filter profile differs by no more than 0.01 mag from the SDSS  $r'$  band (Suberlak *et al.*, 2021) across a wide range of  $g-i$  colour indices. This approach allowed for enhanced temporal coverage and increased the accuracy of the analysis. Since the transient was heavily contaminated by its neighbouring galaxy, we calculated its magnitudes from subtracted images.

We used the ZTF service<sup>3</sup>, which provides difference images in the three ZTF spectral filters. In these

images, the seeing ranges between 1.8 and 2.5 *pixels* (corresponding to 1.8'' and 2.5''). We calculated the target's magnitudes on the subtracted images using aperture photometry with imexam. Following ZTF recommendations, the optimal photometric aperture radius on these frames is approximately 2 *pixels*. We tested this choice on another target observed in ZTF frames with similar seeing conditions, for which ZTF also provides a published PSF-photometry light curve. The comparison showed excellent agreement. For our target, we adopted this aperture size and used only  $r$ -band images, as  $i$ -band images were limited during this observation period. Uncertainties in the ILMT magnitudes were estimated by extrapolating the relation between standard deviation and magnitude for ten nearby non-variable reference stars, with the mean zero-point error of these stars added in quadrature.

Uncertainties in the ZTF magnitudes were estimated from two components: (i) the RMS deviations of the magnitude zero points provided in the ZTF difference image products under the MAGZPRMS keyword, and (ii) the statistical component we calculated from the ZTF difference images, which includes Poisson noise, read-out noise, and background noise (added in quadrature).

The zero points for the ILMT magnitudes were estimated from the science images using a highly photometrically stable nearby star, whose stability was verified against five nearby comparison stars. The zero point used in the ZTF magnitude calculations is provided in the ZTF file headers under the MAGZP keyword.

### 3.2 Results

The resulting lightcurve is presented in Figure 11. It exhibits a decline of approximately 1 magnitude over the first week, followed by a slower fading over the subsequent two weeks. It is important to highlight that the transient was absent in science images prior to April 4th and after May 8th 2024, in data from both the ILMT and the ZTF. This overall light curve morphology, in addition to the spatial association with a classified galaxy, is partially consistent with certain types of supernovae. However, the data are insufficient to exclude alternative interpretations, such as a foreground classical nova. Additional observations across different filters are necessary in order to constrain the nature of this event.

## 4. Conclusions

We have examined CCD frames corresponding to two distinct ILMT fields: Field 0450, starting at  $\alpha_{2000} = 4h$

<sup>3</sup><https://irsa.ipac.caltech.edu/cgi-bin/Gator/nph-scan?projshort=ZTF&mission=irsa>

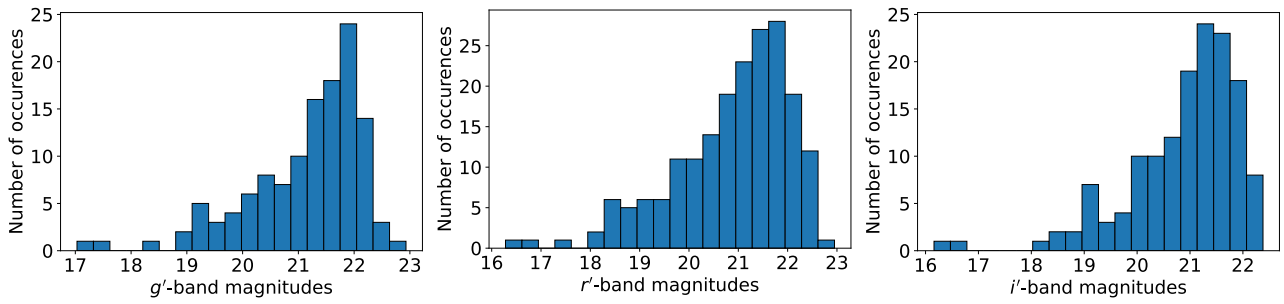


**Figure 9:** Magnitude distribution of the detected asteroids in Field 0450 through the three SDSS filters.

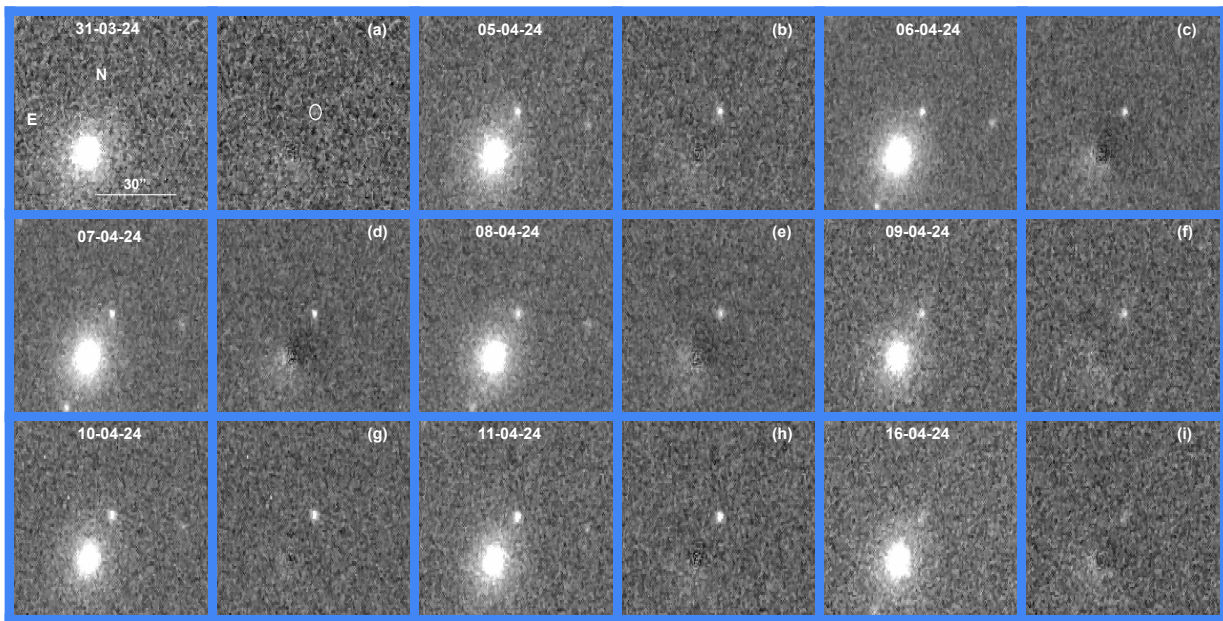


**Figure 10:** Detection of the transient AT 2024fxn in ILMT images. From left to right and top to bottom order, are nine pairs of images, each leftmost (resp. rightmost) representing the science (resp. subtracted) image, where one can see the transient AT 2024fxn near each frame center. In the same order, observation filters are:  $r'$ ,  $r'$ ,  $i'$ ,  $i'$ ,  $i'$ ,  $r'$ ,  $r'$ ,  $r'$ , and  $i'$ .

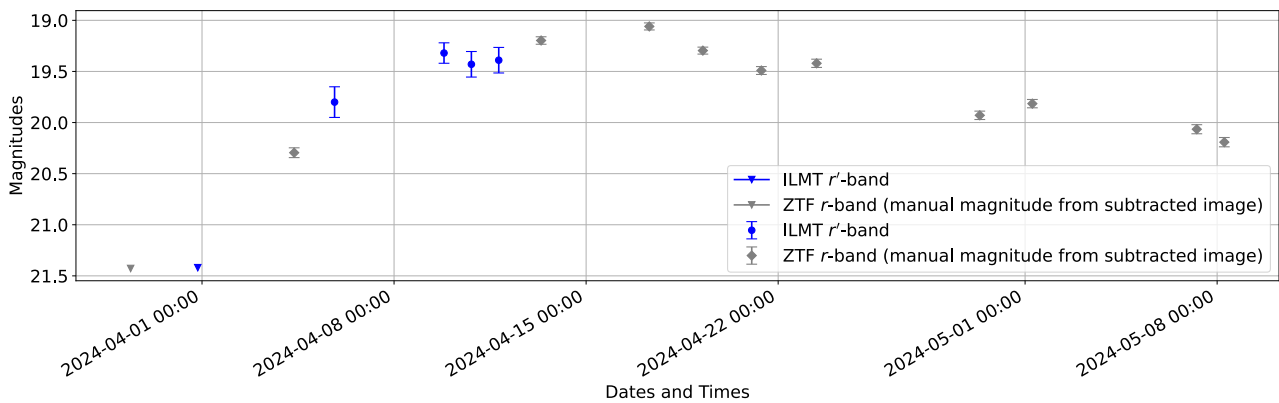


**Figure 11:** Lightcurve of AT 2024fxn based on ILMT and ZTF difference images. Blue symbols represent magnitudes estimated from the ILMT observations, grey represent  $r$ -band magnitudes estimated from ZTF observations, triangles represent magnitude estimates with low statistical significance.

50m and corresponding to low ecliptic and galactic latitudes, and Field 1317, starting at  $\alpha_{2000} = 13\text{h } 17\text{m}$  and corresponding to high ecliptic and galactic latitudes. In Field 0450, we successfully identified 152 distinct asteroids corresponding to 504 detections in total. In Field 1317, we made 30 detections corresponding to 22 unique known MPC asteroids, with one additional detection being a supernova candidate.

We compared the asteroid detectability in these fields for the different SDSS filters. The magnitudes reached in the SDSS  $g'$ ,  $r'$ , and  $i'$  bands under very good seeing and sky transparency conditions are 22.9, 22.9, and 22.4, respectively. The ILMT limiting recall  $V$ -magnitudes using the PyLMT pipeline are 21.5, 22.0, and 22.0 for observations in these respective bands in Field 0450. For Field 1317, these values are 21 for both  $r'$  and  $i'$  bands.

We performed a quantitative comparison between our derived SDSS-band magnitudes and the MPC-predicted  $V$ -band magnitudes for asteroids detected in Field 0450 by fitting a linear relation to the data. This comparison is intended as a diagnostic to validate the photometric calibration of our observations, assess systematic offsets between the SDSS and  $V$  magnitude systems, and evaluate the reliability of the MPC-predicted brightnesses. Fitted slopes are near unity, confirming general consistency, but with large scatter requiring an uncertainty floor of  $\sim 0.32\text{--}0.36$  mag, depending on the filter. This scatter likely reflects systematic effects from MPC  $H$ -magnitude and  $G$ -parameter inaccuracies, uncorrected color terms, and rotational phase differences. The fitted intercepts reveal significant photometric offsets between the two datasets:  $\sim 1.5\text{--}2.1$  mag in  $g'$ ,  $\sim 0.3\text{--}0.5$  mag in  $r'$ , and  $\sim 0.3\text{--}0.4$  mag in  $i'$ . These results highlight the need for caution when using MPC magnitudes in precise photometry, the application of an uncertainty floor of at least 0.3 mag when comparing with catalog predictions, and further investigation of possible color dependencies and rotational modulation effects. Future work will focus on improved color corrections using SDSS colors, phase-angle adjustments, and cross-comparisons with additional surveys such as Pan-STARRS and Gaia.

We verified the agreement between asteroid positions predicted by the MPC and their counterpart measurements with the ILMT. Angular separations between observed and predicted positions of the identified asteroids are consistent with expectations when accounting for the distribution of asteroid angular proper motions and the limited time precision of the MPC cross-checking method. Only a small fraction of cases—four out of the 534 asteroids observed in the two investigated fields—show larger discrepancies and require further investigation.

Future calculated positions might be of importance for enhancing the accuracy of trajectories listed in the MPC database. Calculated magnitudes in the three SDSS bands are of a particular interest for further photometric analysis of these asteroids.

SNe candidates are present among the ILMT data, and are worth follow-up identification. We captured a previously uncatalogued photometric transient in Field 1317 and constructed its lightcurve supplementing the ILMT data with ZTF one. The resulting lightcurve is compatible with a SN-hypothesis, however the rise in flux was rather brief and color information is currently unavailable.

These findings reaffirm the ILMT's efficiency as an excellent asteroid hunter, and a promising extragalactic object identifier, aligning with and complementing prior works (see Pospieszalska-Surdej *et al.* 2024, Pranshu *et al.* 2024, Pranshu *et al.* 2025, Akhunov *et al.* 2024). Additionally, dozens more fields from previous observation cycles are yet to be studied. We expect to detect more asteroids and photometric transients through further examination of these fields and improvements of the pipeline.

## Acknowledgements

The 4-m International Liquid Mirror Telescope (ILMT) project results from a collaboration between the Institute of Astrophysics and Geophysics (University of Liège, Belgium), the Universities of British Columbia, Laval, Montreal, Toronto, Victoria and York, and Aryabhata Research Institute of Observational Sciences (ARIES, India). The authors thank Ankit Bisht, Manisha Kharayat, Hitesh Kumar, Himanshu Rawat, Khushal Singh, Nikhil Dharkiya and other observing staff for their assistance at the 4-m ILMT. The team acknowledges the contributions of ARIES's past and present scientific, engineering and administrative members in the realisation of the ILMT project. JS wishes to thank Service Public Wallonie, F.R.S.-FNRS (Belgium) and the University of Liège, Belgium for funding the construction of the ILMT. PH acknowledges financial support from the Natural Sciences and Engineering Research Council of Canada, RGPIN-2019-04369. SF, PH, AP-S, and JS thank ARIES for hospitality during their visits to Devasthal. KM, BK, BA and ND acknowledge the support from the BRICS grant DST/ICD/BRICS/Call-5/CoNMuTraMO/2023 (G) funded by the DST, India. M.D. acknowledges Innovation in Science Pursuit for Inspired Research (INSPIRE) fellowship award (DST/INSPIRE Fellowship/2020/IF200251) for this work. T.A. thanks Ministry of Higher Education,

Science and Innovations of Uzbekistan (grant FZ-20200929344). JS and KM acknowledge the assistance received from the Anusandhan National Research Foundation (ANRF, SERB- 762 VAJRA Faculty Scheme, India).

This work makes use of data and/or services provided by the International Astronomical Union's Minor Planet Center.

*Software:* Astropy (Astropy Collaboration et al. 2013, 2018, 2022), Matplotlib (Hunter, 2007), NumPy (Harris et al., 2020), imexam (Sosey, 2017), SAOImage DS9 (Joye & Mandel, 2003).

## References

- Akhunov, T., Ailawadhi, B., Borra, E., et al. 2024, Bulletin de la Société Royale des Sciences de Liège, 93, 933, proceedings of the 3rd BINA Workshop on the Scientific Potential of the Indo-Belgian Cooperation
- Bellm, E. C., Kulkarni, S. R., Graham, M. J., et al. 2018, Publications of the Astronomical Society of the Pacific, 131, 018002
- Gibson, B. K., & Hickson, P. 1992, Monthly Notices of the Royal Astronomical Society, 258, 543
- Giorgini, J., Yeomans, D., Chamberlin, A., et al. 1996, in AAS/division for planetary sciences meeting abstracts# 28, Vol. 28, 25–04
- Harris, C. R., Millman, K. J., Van Der Walt, S. J., et al. 2020, Nature, 585, 357
- Hickson, P. 2019, in LPI Contributions, Vol. 2109, First International Orbital Debris Conference, 6066
- Hickson, P., & Richardson, E. H. 1998, Publications of the Astronomical Society of the Pacific, 110, 1081
- Hunter, J. D. 2007, Computing in science & engineering, 9, 90
- Joye, W. A., & Mandel, E. 2003, in Astronomical data analysis software and systems XII, Vol. 295, 489
- Juric, M., Ivezić, Z., Lupton, R. H., et al. 2002, ASTRONOMICAL JOURNAL-AMERICAN ASTRONOMICAL SOCIETY, 124, 1776
- Magnier, E. A., Chambers, K., Flewelling, H., et al. 2020, The Astrophysical Journal Supplement Series, 251, 3
- Pospieszalska-Surdej, A., Ailawadhi, B., Akhunov, T., et al. 2024, Bulletin de la Société Royale des Sciences de Liège, 93, 941–947, proceedings of the 3rd BINA Workshop on the Scientific Potential of the Indo-Belgian Cooperation
- Pranshu, K., Ailawadhi, B., Akhunov, T., et al. 2024, Bulletin de la Société Royale des Sciences de Liège, 93, 828–836, proceedings of the 3rd BINA Workshop on the Scientific Potential of the Indo-Belgian Cooperation
- Pranshu, K., Misra, K., Ailawadhi, B., et al. 2024, Transient Name Server Discovery Report, 2024-964, 1
- Pranshu, K., Misra, K., Ailawadhi, B., et al. 2025, Monthly Notices of the Royal Astronomical Society, 538, 133
- Pravec, P., Harris, A. W., Kušnirák, P., Galád, A., & Hornoch, K. 2012, Icarus, 221, 365
- Price-Whelan, A. M., Sipőcz, B., Günther, H., et al. 2018, The Astronomical Journal, 156, 123
- Sosey, M. 2017, Zenodo
- Suberlak, K. L., Ivezić, Ž., & MacLeod, C. 2021, The Astrophysical Journal, 907, 96
- Surdej, J., Hickson, P., Borra, H., et al. 2018, Bulletin de la Société Royale des Sciences de Liège, 87, 68
- Surdej, J., Ailawadhi, B., Akhunov, T., et al. 2024, Bulletin de la Société Royale des Sciences de Liège, 93, 1054
- Surdej, J., Hickson, P., Misra, K., et al. 2025, Astronomy & Astrophysics, 694, A80
- Tonry, J., Denneau, L., Heinze, A., et al. 2018, Publications of the Astronomical Society of the Pacific, 130, 064505
- Vereš, P., Jedicke, R., Fitzsimmons, A., et al. 2015, Icarus, 261, 34

## Appendix A Detection classes

We classified the detected asteroids according to different detection classes:

- MP: The asteroid appears in the MPC, and was detected by the CNN algorithm.
- MN: The asteroid appears in the MPC, and was detected visually.
- MNBS: The asteroid appears in the MPC, was detected visually near a Bright Star, and was not detected by the CNN algorithm due to the angular proximity to that Bright Star.
- MNF: The asteroid appears in the MPC, and was detected visually, but is Faint.
- MNVF: The asteroid appears in the MPC, and was detected visually, but is Very Faint.
- MN-MP: The asteroid was detected by the CNN algorithm after tuning its parameters.

## Appendix B Photometry parameters

Asteroid magnitudes are estimated through aperture photometry. The catalogues and band-passes used for the calibrators are:

- For the *r*'-band detections: *The Guide Star Catalog, Version 2.4.2 (GSC2.4.2) (STScI, 2020), rmag values (SDSS r-band).*
- For the *g*'-band detections: *The Guide Star Catalog, Version 2.4.2 (GSC2.4.2) (STScI, 2020), gmag values (SDSS g-band).*
- For the *i*'-band detections: *The Guide Star Catalog, Version 2.4.2 (GSC2.4.2) (STScI, 2020), imag values (SDSS i-band).*

Note: The magnitude uncertainties are estimated based upon the zero point variations and are intended to reflect the stability of the photometric calibration. Generally, this zero point uncertainty is smaller than 0.1 mag; otherwise, a note is provided in the table's rightmost column. Unless specified otherwise, a minimum of three neighbouring stars has been used to estimate the zero point. The full photometric uncertainty budget is described in Section 2.2. Measurements flagged with ':' or '::' indicate high photometric uncertainty and are excluded from the analysis described in Section 2.2.

## Appendix C Asteroid detection tables

### Description of the tables

Tables 2 and 3 present the asteroids found in Field 0450 and at  $\alpha = 13^{\text{h}} 17^{\text{m}}$ , respectively. The different targets were sorted following the order of their increasing right ascension.

Table 2 contains: date and time of observation, J2000.0 equatorial coordinates predicted by the MPC, angular distance between MPC-predicted and ILMT-observed positions, MPC-predicted V magnitude, MPC name, ILMT detection class, filter used for ILMT observation (F), J2000.0 equatorial coordinates observed by the ILMT, ILMT photometry in the given filter, type of photometry (Flag), and Notes.

The cited filters are from the SDSS. 'Flag' specifies the method used to calculate the magnitude and/or position: 'pho1' refers to the *statistical* method, 'pho2' to the *individualised* method, and 'pho3' to a position estimate derived from the CNN algorithm, based on visual examination rather than centroid fitting. The 'Notes' column provides further information about the aperture photometry parameters and is further developed in Appendix E.

In Table 3 we present the same columns as in Table 2, with the exception of the 'Notes' column.

Table C.1: List of asteroids detected in the field starting at  $\alpha = 4\text{h } 50\text{m}$ .

<i>Date</i>	<i>Time(UT1)</i>	<i>RA(hms)</i>	<i>Dec(dms)</i>	<i>Dist(″)</i>	<i>Mag(V)</i>	<i>Name</i>	<i>Class</i>	<i>F</i>	<i>RA<sub>det</sub></i>	<i>Dec<sub>det</sub></i>	<i>Mag<sub>det</sub></i>	<i>Flag</i>	<i>Notes</i>
20221024	21:19:17	04 49 36.9	+29 23 00	0.53	20.8	2022 WW3	MIN-MP	r	04:49:36.86	+29:23:00.1	19.91:	pho1	c
20221024	21:19:23	04 49 42.8	+29 17 59	0.24	21.9	2013 CF133	MIN	r	04:49:42.81	+29:17:59.2	22.25	pho1	
20221024	21:19:27	04 49 46.7	+29 19 39	0.49	21.8	2008 UH219	MIN	r	04:49:46.67	+29:19:38.7	21.21	pho1	
20221024	21:19:34	04 49 53.6	+29 23 01	0.64	22.3	2019 AV73	MINVF	r	04:49:53.57	+29:23:01.5	21.94	pho2	
20221024	21:19:42	04 50 01.4	+29 28 38	0	20.7	2002 TN98	MP	r	04:50:01.40	+29:28:38.0	20.65	pho1	
20221024	21:19:43	04 50 02.5	+29 25 15	0.39	20.8	2001 SR103	MP	r	04:50:02.47	+29:25:15.0	21.25	pho1	
20221024	21:20:23	04 50 43.3	+29 09 27	0.84	22.3	2017 UG118	MINVF	r	04:50:43.28	+29:09:27.8	22.1	pho2	
20221024	21:20:24	04 50 43.8	+29 15 35	0	21.8	2006 UM267	MIN-MP	r	04:50:43.80	+29:15:35.0	21.68	pho1	
20221024	21:20:37	04 50 56.7	+29 15 55	0.4	21.5	2016 WK13	MINVF	r	04:50:56.68	+29:15:54.7	21.3	pho1	
20221024	21:20:59	04 51 19.3	+29 20 47	0.52	21.0	2008 CY138	MP	r	04:51:19.31	+29:20:47.5	20.77:	pho2	c+
20221024	21:21:27	04 51 48.4	+29 09 01	1.11	22.2	2008 TS76	MINVF	r	04:51:48.41	+29:09:02.1	22.15	pho1	
20221024	21:21:59	04 52 19.5	+29 22 43	0.16	21.2	2011 SS235	MP	r	04:52:19.51	+29:22:43.1	21.65	pho1	
20221024	21:22:21	04 52 42.2	+29 15 52	1.51	22.5	2022 UR93	MINVF	r	04:52:42.19	+29:15:50.5	21.96	pho1	
20221024	21:22:26	04 52 46.7	+29 14 46	3.09	20.1	2018 TJ	MINBS	r	04:52:46.88	+29:14:44.0	18.92	pho1	
20221024	21:22:37	04 52 58.1	+29 07 59	0.61	20	2001 YE46	MP	r	04:52:58.09	+29:07:59.6	20.01	pho1	
20221024	21:22:41	04 53 01.9	+29 11 21	0.48	21.8	2015 XX362	MIN-MP	r	04:53:01.88	+29:11:21.4	21.66	pho1	
20221024	21:23:08	04 53 29.4	+29 09 01	0.75	21.4	2015 CP64	MP	r	04:53:29.38	+29:09:01.7	21.79	pho1	
20221024	21:23:14	04 53 34.5	+29 17 35	0.92	21.5	2009 SH359	MP	r	04:53:34.43	+29:17:34.9	21.86	pho1	
20221024	21:23:18	04 53 39.3	+29 14 58	0.28	20.8	2011 UN326	MP	r	04:53:39.28	+29:14:58.1	21.03	pho1	
20221024	21:23:20	04 53 41.1	+29 27 35	1.54	21.6	2006 QH207	MIN-MP	r	04:53:41.01	+29:27:36.0	21.42	pho1	
20221024	21:23:27	04 53 48.1	+29 19 46	1.75	21.4	2008 UM37	MIN-MP	r	04:53:47.99	+29:19:47.0	21.54	pho1	
20221024	21:23:33	04 53 54.0	+29 25 53	1.45	21.5	2012 TC44	MINBS	r	04:53:53.95	+29:25:54.3	nomag	pho2	c++
20221024	21:23:51	04 54 11.8	+29 09 29	0.91	21.7	2014 YW98	MIN-MP	r	04:54:11.79	+29:09:29.9	21.23	pho1	
20221024	21:23:55	04 54 16.0	+29 12 35	2.24	18.8	2002 JY112	MP	r	04:54:15.88	+29:12:33.4	18.6	pho1	
20221024	21:23:56	04 54 16.6	+29 12 12	0.84	21	2006 SP312	MP	r	04:54:16.58	+29:12:12.8	20.92	pho1	
20221024	21:23:56	04 54 17.2	+29 19 30	0.72	20	2001 TK10	MP	r	04:54:17.15	+29:19:30.3	19.56	pho1	
20221024	21:24:13	04 54 33.6	+29 25 42	1.7	20.9	2005 GN93	MP	r	04:54:33.49	+29:25:42.9	20.74	pho1	
20221024	21:24:28	04 54 48.8	+29 26 53	1.26	17.6	2000 OD48	MP	r	04:54:48.72	+29:26:53.7	17.41	pho1	
20221024	21:24:33	04 54 54.3	+29 21 56	0.9	21.5	2004 MF9	MINBS	r	04:54:54.3	+29:21:55.1	nomag	pho2	c++
20221024	21:24:38	04 54 59.1	+29 12 21	0.56	20.8	2007 DX78	MP	r	04:54:59.07	+29:12:21.4	20.74	pho1	
20221024	21:25:51	04 56 12.1	+29 20 15	1.16	19.5	1999 XB132	MP	r	04:56:12.02	+29:20:15.5	19.31	pho1	
20221024	21:26:02	04 56 22.8	+29 13 56	3.2	19	2001 TP105	MP	r	04:56:22.79	+29:13:59.2	19.04	pho1	

continued.

<i>Date</i>	<i>Time(UT1)</i>	<i>RA(hms)</i>	<i>Dec(dms)</i>	<i>Dist(°)</i>	<i>Mag(V)</i>	<i>Name</i>	<i>Class</i>	<i>F</i>	<i>RA<sub>det</sub></i>	<i>Dec<sub>det</sub></i>	<i>Mag<sub>det</sub></i>	<i>Flag</i>	<i>Notes</i>
20221024	21:26:14	04 56 34.7	+29 14 47	1.65	20.7	2002 JF147	MP	r	04:56:34.6	+29:14:48	nomag	none	c++
20221024	21:26:18	04 56 39.3	+29 21 03	1.52	20.2	1997 TW23	MP	r	04:56:39.22	+29:21:04.1	20	pho1	
20221024	21:26:20	04 56 40.8	+29 17 37	1.9	19.7	2002 CM221	MP	r	04:56:40.66	+29:17:37.5	19.33	pho1	
20221024	21:26:37	04 56 58.2	+29 11 50	0.94	19.5	2001 VP14	MP	r	04:56:58.13	+29:11:50.2	20.18	pho1	
20221024	21:26:41	04 57 02.0	+29 15 38	0.24	21.6	2015 FD78	MNVF	r	04:57:01.99	+29:15:38.2	22.11	pho1	
20221024	21:26:45	04 57 05.4	+29 25 32	1.44	21.5	2010 VW257	MN-MP	r	04:57:05.29	+29:25:32.0	21.4	pho2	
20221024	21:26:56	04 57 16.9	+29 29 23	1.92	22.2	2016 ED307	MN	r	04:57:16.76	+29:29:23.6	21.57	pho2	
20221024	21:27:03	04 57 23.7	+29 23 06	1.65	20.1	2004 TG158	MP	r	04:57:23.59	+29:23:06.8	19.86	pho1	
20221024	21:27:08	04 57 29.2	+29 13 10	1.26	21.4	2015 MX19	MN-MP	r	04:57:29.12	+29:13:10.7	21.21	pho1	
20221024	21:27:10	04 57 31.2	+29 24 42	1.84	21.5	2016 TZ33	MP	r	04:57:31.06	+29:24:42.2	22.22	pho1	
20221024	21:27:14	04 57 35.1	+29 27 40	1.97	20.9	2010 KX14	MP	r	04:57:34.95	+29:27:40.2	20.72	pho1	
20221024	21:27:18	04 57 39.1	+29 29 35	1.67	21.6	2008 TR135	MN	r	04:57:39.03	+29:29:36.4	22.33	pho1	
20221024	21:27:26	04 57 46.8	+29 22 32	1.26	21.6	2010 RP92	MP	r	04:57:46.72	+29:22:31.3	21.59	pho1	
20221024	21:27:30	04 57 50.7	+29 23 08	1.65	20.4	2001 XK231	MP	r	04:57:50.58	+29:23:07.5	nomag	pho1	c++
20221024	21:27:31	04 57 52.9	+29 12 13	1.18	21.1	2008 OX22	MP	r	04:57:52.81	+29:12:12.9	20.89	pho1	
20221024	21:27:31	04 57 53.0	+29 15 36	2.16	21.4	2006 DH80	MP	r	04:57:52.85	+29:15:36.9	21.42	pho1	
20221024	21:28:29	04 58 51.2	+29 21 34	1.28	21.3	2014 NT70	MP	r	04:58:51.11	+29:21:34.5	21.48	pho1	
20221024	21:28:39	04 59 00.7	+29 22 57	0.9	21.9	2015 TQ55	MN	r	04:59:00.70	+29:22:57.9	21.72	pho2	
20221024	21:29:06	04 59 27.8	+29 24 54	0.72	21.7	2019 AG42	MN-MP	r	04:59:27.84	+29:24:53.5	21.68	pho1	
20221024	21:29:12	04 59 33.4	+29 08 10	0.65	22.8	2009 SO42	MNVF	r	04:59:33.42	+29:08:10.6	22.03	pho2	ext 2*
20221024	21:29:16	04 59 37.4	+29 22 09	0.42	22	2016 TY181	MNVF	r	04:59:37.41	+29:22:08.6	21.9	pho2	ext 2*
20221024	21:29:25	04 59 46.6	+29 10 04	1.64	18.7	2002 DN7	MP	r	04:59:46.65	+29:10:02.5	18.44	pho1	
20221024	21:29:56	05 00 18.1	+29 09 12	0.92	20	2011 BJ132	MP	r	05:00:18.03	+29:09:11.9	19.95	pho1	
20221024	21:30:31	05 00 53.0	+29 28 08	1.26	21.3	2022 SX246	MP	r	05:00:52.97	+29:28:06.8	21.15	pho1	
20221024	21:30:32	05 00 53.5	+29 15 42	3.04	23.1	2008 SK43	MNVF	r	05:00:53.73	+29:15:42.4	22.25	pho1	
20221024	21:30:34	05 00 55.9	+29 09 18	0.72	21.3	2011 JK10	MP	r	05:00:55.95	+29:09:17.7	21.16	pho1	
20221024	21:30:36	05 00 57.5	+29 21 04	0.87	20.6	2014 RD50	MP	r	05:00:57.54	+29:21:03.3	20.47	pho1	
20221024	21:30:36	05 00 58.1	+29 22 28	0.56	20.9	2002 CW77	MP	r	05:00:58.13	+29:22:27.6	20.17	pho1	
20221024	21:30:46	05 01 08.1	+29 09 37	0.99	21.5	2008 XL25	MN-MP	r	05:01:08.16	+29:09:36.4	22.34	pho1	
20221024	21:31:12	05 01 33.3	+29 21 54	0.4	21.6	2016 QY110	MN	r	05:01:33.33	+29:21:54.1	21.35	pho1	
20221024	21:31:19	05 01 40.5	+29 18 01	1	21.6	2009 UZ18	MN	r	05:01:40.57	+29:18:00.6	21.97	pho1	
20221024	21:31:29	05 01 50.6	+29 10 34	0.72	22.2	2015 BB420	MNVF	r	05:01:50.65	+29:10:34.3	22.04	pho1	

continued.

<i>Date</i>	<i>Time(UT1)</i>	<i>RA(hms)</i>	<i>Dec(dms)</i>	<i>Dist(")</i>	<i>Mag(V)</i>	<i>Name</i>	<i>Class</i>	<i>F</i>	<i>RA<sub>det</sub></i>	<i>Dec<sub>det</sub></i>	<i>Mag<sub>det</sub></i>	<i>Flag</i>	<i>Notes</i>
20221024	21:31:40	05 02 01.3	+29 20 58	0.33	19.8	2001 QO36	MP	r	05:02:01.32	+29:20:57.8	18.43:	pho1	c
20221024	21:32:00	05 02 21.2	+29 28 06	0.33	20.3	2005 WT71	MP	r	05:02:21.22	+29:28:05.8	20.53	pho1	
20221024	21:32:36	05 02 57.3	+29 16 55	0	20.7	2004 GC42	MP	r	05:02:57.30	+29:16:55.0	20.82	pho1	
20221024	21:32:42	05 03 03.5	+29 18 35	1	21.5	2015 JO14	MP	r	05:03:03.50	+29:18:34.0	20.95	pho1	
20221024	21:32:50	05 03 11.6	+29 15 00	0.48	22.4	2015 BE609	MNVF	r	05:03:11.58	+29:15:00.4	22.5	pho1	
20221024	21:33:00	05 03 21.9	+29 27 10	0.93	22.1	2007 RJ344	MP	r	05:03:21.84	+29:27:09.5	nomag	none	c++
20221024	21:33:03	05 03 25.2	+29 16 15	0.42	21.2	2013 EE66	MP	r	05:03:25.21	+29:16:15.4	21.25	pho1	
20221024	21:33:24	05 03 45.4	+29 24 01	0.4	22.3	2012 RF39	MNVF	r	05:03:45.38	+29:24:01.3	21.96	pho1	
20221024	21:33:30	05 03 51.5	+29 14 50	0.79	18.7	Melanthios	MP	r	05:03:51.56	+29:14:49.9	18.61	pho1	
20221024	21:33:36	05 03 59.0	+29 23 48	0.49	21	2008 SP198	MP	r	05:03:58.97	+29:23:48.3	21.16	pho1	
20221024	21:33:55	05 04 17.2	+29 24 22	0.3	20.1	2003 UV192	MP	r	05:04:17.20	+29:24:22.3	20.14	pho1	
20221024	21:34:12	05 04 34.9	+29 20 56	0.24	21.5	2012 TB	P	r	05:04:34.91	+29:20:56.2	21.46	pho1	
20221024	21:34:16	05 04 38.4	+29 20 23	0.13	18	1990 QQ4	MP	r	05:04:38.41	+29:20:23.0	18.17	pho1	
20221025	21:15:08	04 49 23.5	+29 18 44	0.49	21.9	2013 CF133	MIN	r	04:49:23.53	+29:18:43.7	21.81	pho1	
20221025	21:15:17	04 49 33.0	+29 24 08	0.52	20.8	2022 WW3	MIN	r	04:49:33.04	+29:24:08.0	20.44	pho1	
20221025	21:15:30	04 49 45.3	+29 27 51	1.21	20.8	2001 SR103	MP	r	04:49:45.39	+29:27:50.7	20.89	pho1	
20221025	21:16:01	04 50 17.0	+29 19 05	1.27	21.8	2006 UM267	MIN	r	04:50:17.06	+29:19:04.0	22.17	pho1	
20221025	21:16:04	04 50 19.7	+29 24 25	0.82	22.4	2015 BB404	MNVF	r	04:50:19.75	+29:24:25.5	21.49	pho1	
20221025	21:16:04	04 50 20.0	+29 10 10	1.31	22.3	2017 UG118	MNVF	r	04:50:20.1	+29:10:10.1	22.53:	pho2	ext
20221025	21:16:15	04 50 31.3	+29 20 30	0.93	21.5	2016 WK13	MIN	r	04:50:31.36	+29:20:29.5	21.62	pho1	
20221025	21:16:22	04 50 37.9	+29 16 02	0.77	22.3	2014 FB73	MIN	r	04:50:37.95	+29:16:01.6	22.59	pho1	
20221025	21:16:45	04 51 00.5	+29 23 13	0.66	21	2008 CY138	MP	r	04:51:00.55	+29:23:12.9	20.87	pho1	
20221025	21:16:56	04 51 12.3	+29 19 46	1.34	21.5	2003 SW454	MIN	r	04:51:12.4	+29:19:46.3	nomag	pho2	c++
20221025	21:17:10	04 51 26.4	+29 14 19	0.44	22.5	2020 RA126	MIN	r	04:51:26.43	+29:14:18.8	22.41	pho1	
20221025	21:17:12	04 51 28.3	+29 10 54	0.56	20.6	2004 TL61	MP	r	04:51:28.34	+29:10:53.8	20.47	pho1	
20221025	21:17:13	04 51 29.1	+29 09 59	1.49	22.2	2008 TS76	MNVF	r	04:51:29.20	+29:09:58.3	21.95	pho1	
20221025	21:17:45	04 52 00.7	+29 21 30	0.68	21.1	2011 SS235	MP	r	04:52:00.75	+29:21:30.2	22.13	pho1	
20221025	21:18:17	04 52 34.3	+29 24 55	1.62	22.5	2017 DO128	MNVF	r	04:52:34.18	+29:24:55.4	22.3	pho2	
20221025	21:18:29	04 52 46.1	+29 28 35	1.4	21	2015 BQ42	MP	r	04:52:46.10	+29:28:36.4	20.82	pho1	
20221025	21:18:33	04 52 49.5	+29 17 18	1.07	21.5	2014 XM21	MIN	r	04:52:49.53	+29:17:19.0	21.67	pho1	
20221025	21:18:47	04 53 03.8	+29 10 06	1	21.4	2015 CP64	MIN-MP	r	04:53:03.8	+29:10:07	nomag	none	c++
20221025	21:18:48	04 53 05.1	+29 19 14	0.68	21.5	2009 SH359	MIN-MP	r	04:53:05.15	+29:19:14.2	21.52	pho1	

continued.

<i>Date</i>	<i>Time(UT1)</i>	<i>RA(hms)</i>	<i>Dec(dms)</i>	<i>Dist(°)</i>	<i>Mag(V)</i>	<i>Name</i>	<i>Class</i>	<i>F</i>	<i>RA<sub>det</sub></i>	<i>Dec<sub>det</sub></i>	<i>Mag<sub>det</sub></i>	<i>Flag</i>	<i>Notes</i>
20221025	21:18:48	04 53 05.4	+29 17 42	0.6	21.8	2015 XX362	MNVF	r	04:53:05.36	+29:17:41.7	22.16	pho1	
20221025	21:19:05	04 53 21.8	+29 29 54	0.87	21.6	2006 QH207	MP	r	04:53:21.76	+29:29:54.7	21.52	pho1	
20221025	21:19:11	04 53 28.2	+29 25 44	0.6	21.4	2008 UM37	MP	r	04:53:28.20	+29:25:43.4	21.19	pho1	
20221025	21:19:14	04 53 30.7	+29 26 08	0.91	21.5	2012 TC44	MN-MP	r	04:53:30.77	+29:26:08.0	21.32	pho1	
20221025	21:19:16	04 53 32.8	+29 12 13	0	20.8	2011 UN326	MP	r	04:53:32.80	+29:12:13.0	20.5	pho1	
20221025	21:19:33	04 53 50.0	+29 13 11	0.41	21.7	2014 YW98	MN-MP	r	04:53:50.03	+29:13:11.1	21.41	pho1	
20221025	21:19:37	04 53 53.8	+29 23 13	0.24	20	2001 TK10	MP	r	04:53:53.79	+29:23:13.2	19.73	pho1	
20221025	21:19:39	04 53 56.0	+29 18 27	0.24	20.9	2006 SP312	MP	r	04:53:56.01	+29:18:27.2	20.83	pho1	
20221025	21:19:58	04 54 14.6	+29 28 27	1.11	20.9	2005 GN93	MP	r	04:54:14.61	+29:28:28.1	20.67	pho1	
20221025	21:20:12	04 54 29.0	+29 30 08	0.6	17.6	2000 OD48	MIN	r	04:54:28.96	+29:30:08.3	16.81:	pho1	c++
20221025	21:20:15	04 54 31.7	+29 19 37	0.7	21.5	2004 MF9	MNVF	r	04:54:31.70	+29:19:36.3	22.49	pho1	
20221025	21:20:26	04 54 43.1	+29 15 36	0.49	20.8	2007 DX78	MP	r	04:54:43.13	+29:15:36.3	20.51	pho1	
20221025	21:20:52	04 55 08.7	+29 17 10	0.4	22	2013 JK15	MNVF	r	04:55:08.68	+29:17:09.7	21.97	pho2	
20221025	21:20:55	04 55 11.5	+29 17 47	0.3	22.5	2021 QQ71	MNVF	r	04:55:11.50	+29:17:47.3	22	pho2	ext
20221025	21:21:36	04 55 52.6	+29 22 34	0.68	19.5	1999 XB132	MP	r	04:55:52.55	+29:22:33.8	19.21	pho1	
20221025	21:21:47	04 56 03.9	+29 15 37	0.99	20.7	2002 JF147	MP	r	04:56:03.84	+29:15:37.6	20.39	pho1	
20221025	21:21:47	04 56 04.2	+29 24 22	1.45	18.9	2001 TP105	MP	r	04:56:04.17	+29:24:23.4	18.9	pho1	
20221025	21:21:54	04 56 10.5	+29 25 22	1.03	20.1	1997 TW23	MP	r	04:56:10.45	+29:25:22.8	20.08	pho1	
20221025	21:21:57	04 56 13.6	+29 21 07	0.64	19.7	2002 CM221	MP	r	04:56:13.57	+29:21:07.5	19.73	pho1	
20221025	21:22:25	04 56 42.4	+29 12 04	1	19.5	2001 VP14	MP	r	04:56:42.33	+29:12:04.4	19.26	pho1	
20221025	21:22:27	04 56 43.7	+29 17 02	0.56	21.5	2015 FD78	MIN	r	04:56:43.67	+29:17:01.6	21.29	pho1	
20221025	21:22:32	04 56 48.3	+29 25 32	0.64	21.5	2010 VW257	MP	r	04:56:48.27	+29:25:32.5	22.54	pho1	
20221025	21:22:32	04 56 49.2	+29 27 59	2.83	22.2	2016 ED307	MNVF	r	04:56:49.0	+29:27:57.9	nomag	none	c++
20221025	21:22:47	04 57 04.1	+29 25 35	0.4	20.1	2004 TG158	MP	r	04:57:04.08	+29:25:35.3	19.91	pho1	
20221025	21:22:52	04 57 08.8	+29 24 03	1.32	21.5	2016 TZ33	MP	r	04:57:08.70	+29:24:03.2	21.81	pho1	
20221025	21:22:53	04 57 10.2	+29 15 47	0.93	21.4	2015 MX19	MNBS	r	04:57:10.14	+29:15:47.5	nomag	pho2	c++
20221025	21:22:56	04 57 12.4	+29 27 04	1.19	20.9	2010 KX14	MP	r	04:57:12.31	+29:27:03.8	20.68	pho1	
20221025	21:23:10	04 57 27.1	+29 16 54	0.93	21.4	2006 DH80	MP	r	04:57:27.04	+29:16:53.5	20.54	pho1	
20221025	21:23:11	04 57 27.7	+29 21 18	0.8	21.6	2010 RP92	MNBS	r	04:57:27.7	+29:21:17.2	nomag	none	c++
20221025	21:23:11	04 57 27.8	+29 22 35	0.4	20.4	2001 XK231	MP	r	04:57:27.80	+29:22:34.6	20.22	pho1	
20221025	21:23:18	04 57 34.8	+29 12 37	0.92	21.1	2008 OX22	MP	r	04:57:34.73	+29:12:37.1	20.61	pho1	
20221025	21:23:55	04 58 12.3	+29 22 59	0.92	22.1	2010 CZ29	MNVF	r	04:58:12.23	+29:22:58.9	22.53	pho1	

continued.

<i>Date</i>	<i>Time(UT1)</i>	<i>RA(hms)</i>	<i>Dec(dms)</i>	<i>Dist(")</i>	<i>Mag(V)</i>	<i>Name</i>	<i>Class</i>	<i>F</i>	<i>RA<sub>det</sub></i>	<i>Dec<sub>det</sub></i>	<i>Mag<sub>det</sub></i>	<i>Flag</i>	<i>Notes</i>
20221025	21:24:02	04 58 19.2	+29 08 03	1.99	22	2015 VX90	MNVF	<i>r</i>	04:58:19.10	+29:08:04.5	21.68	pho1	
20221025	21:24:05	04 58 21.9	+29 17 24	1.43	23.6	1998 SJ70	MNVF	<i>r</i>	04:58:21.96	+29:17:25.2	22.95	pho2	ld
20221025	21:24:22	04 58 39.4	+29 22 13	0.72	21.2	2014 NT70	MP	<i>r</i>	04:58:39.35	+29:22:13.3	21.06	pho1	
20221025	21:24:42	04 58 59.5	+29 24 43	0.4	21.8	2015 TQ55	MN-MP	<i>r</i>	04:58:59.48	+29:24:42.7	21.59	pho1	
20221025	21:24:51	04 59 08.4	+29 25 43	1.58	21.7	2019 AG42	MP	<i>r</i>	04:59:08.28	+29:25:43.2	21.77	pho1	
20221025	21:24:58	04 59 16.0	+29 25 49	2	22	2016 TY181	MIN	<i>r</i>	04:59:15.85	+29:25:49.4	21.75	pho2	ext
20221025	21:25:10	04 59 27.8	+29 18 46	2.01	18.6	2002 DN7	MP	<i>r</i>	04:59:27.75	+29:18:47.9	18.66	pho1	
20221025	21:26:11	05 00 28.7	+29 11 17	1.27	21.3	2011 JK10	MP	<i>r</i>	05:00:28.64	+29:11:18.0	21.01	pho1	
20221025	21:26:17	05 00 35.0	+29 09 50	0.66	20	2011 BJ132	MP	<i>r</i>	05:00:35.05	+29:09:49.9	20.18	pho1	
20221025	21:26:21	05 00 39.1	+29 25 10	1.88	20.6	2014 RD50	MP	<i>r</i>	05:00:38.97	+29:25:10.8	20.41	pho1	
20221025	21:26:23	05 00 40.8	+29 12 23	1.61	21.5	2008 XL25	MP	<i>r</i>	05:00:40.71	+29:12:24.1	21.75	pho1	
20221025	21:26:23	05 00 40.9	+29 24 38	1.04	20.8	2002 CW77	MP	<i>r</i>	05:00:40.83	+29:24:38.5	21.09	pho1	
20221025	21:26:44	05 01 00.6	+29 14 11	2.5	21.4	2022 SZ296	MP	<i>r</i>	05:01:00.61	+29:14:13.5	20	pho2	
20221025	21:27:06	05 01 23.5	+29 19 35	1.03	21.6	2009 UZ18	MP	<i>r</i>	05:01:23.45	+29:19:35.8	21.44	pho1	
20221025	21:27:16	05 01 34.1	+29 12 12	1.37	22.2	2015 BB420	MNVF	<i>r</i>	05:01:34.00	+29:12:12.4	22.43	pho1	
20221025	21:27:28	05 01 45.7	+29 22 16	1	19.8	2001 QO36	MP	<i>r</i>	05:01:45.63	+29:22:16.4	19.7	pho1	
20221025	21:27:37	05 01 54.6	+29 27 56	2.11	21.3	2010 AM166	MP	<i>r</i>	05:01:54.76	+29:27:55.7	20.86	pho1	
20221025	21:27:44	05 02 01.9	+29 30 16	1.99	20.3	2005 WT71	MP	<i>r</i>	05:02:01.80	+29:30:17.5	19.81	pho1	
20221025	21:28:20	05 02 38.1	+29 20 35	1.72	20.7	2004 GC42	MP	<i>r</i>	05:02:37.98	+29:20:35.7	20.47	pho1	
20221025	21:28:23	05 02 40.7	+29 21 50	3.23	21.5	2015 JO14	MP	<i>r</i>	05:02:40.49	+29:21:51.7	21.06	pho1	
20221025	21:28:36	05 02 53.7	+29 09 43	2.78	20.5	2000 SQ115	MP	<i>r</i>	05:02:53.57	+29:09:45.2	19.94	pho1	
20221025	21:28:47	05 03 04.5	+29 15 23	1.09	21.2	2013 EE66	MP	<i>r</i>	05:03:04.42	+29:15:22.7	21.53	pho1	
20221025	21:28:48	05 03 05.8	+29 29 28	2.04	22.1	2007 RJ344	MN-MP	<i>r</i>	05:03:05.66	+29:29:28.9	21.5	pho1	
20221025	21:29:17	05 03 34.5	+29 15 43	0.53	18.6	Melanthios	MP	<i>r</i>	05:03:34.54	+29:15:42.9	18.59	pho1	
20221025	21:29:25	05 03 42.4	+29 23 38	0.77	20.9	2008 SP198	MP	<i>r</i>	05:03:42.45	+29:23:37.6	21.71	pho1	
20221025	21:29:45	05 04 02.4	+29 25 47	0.24	20.1	2003 UV192	MP	<i>r</i>	05:04:02.41	+29:25:47.2	19.84	pho1	
20221025	21:29:55	05 04 12.5	+29 24 09	0.4	21.4	2012 TB	P	<i>r</i>	05:04:12.52	+29:24:08.7	21.81	pho1	
20221025	21:30:00	05 04 17.9	+29 09 52	0.5	19.4	2001 TN65	MP	<i>r</i>	05:04:17.90	+29:09:51.5	18.98	pho1	
20221025	21:30:01	05 04 18.5	+29 23 58	0.65	18	1990 QQ4	MP	<i>r</i>	05:04:18.52	+29:23:57.4	18.23	pho1	
20221025	21:30:03	05 04 20.5	+29 14 21	0.89	19.4	2000 HF12	MP	<i>r</i>	05:04:20.55	+29:14:20.4	18.87	pho1	
20221025	21:30:18	05 04 36.9	+29 24 59	0.84	21.7	2015 FA186	MP	<i>r</i>	05:04:36.92	+29:24:59.8	21.78	pho1	
20221026	21:11:37	04 49 48.9	+29 22 30	2.4	21.8	2006 UM267	MNVF	<i>g</i>	04:49:48.73	+29:22:30.9	22.39	pho2	2-*

continued.

<i>Date</i>	<i>Time(UT1)</i>	<i>RA(hms)</i>	<i>Dec(dms)</i>	<i>Dist(°)</i>	<i>Mag(V)</i>	<i>Name</i>	<i>Class</i>	<i>F</i>	<i>RA<sub>det</sub></i>	<i>Dec<sub>det</sub></i>	<i>Mag<sub>det</sub></i>	<i>Flag</i>	<i>Notes</i>
20221026	21:11:53	04 50 04.5	+29 25 00	1.45	21.4	2016 WK13	MNVF	<i>g</i>	04:50:04.42	+29:25:01.0	21.4	pho2	0.13
20221026	21:12:28	04 50 40.1	+29 25 33	1.99	21	2008 CY138	MNVF	<i>g</i>	04:50:40.01	+29:25:34.6	21.85	pho1	
20221026	21:12:37	04 50 49.6	+29 18 47	2.26	21.5	2003 SW454	MNVF	<i>g</i>	04:50:49.43	+29:18:46.6	21.4	pho2	byh
20221026	21:12:45	04 50 57.5	+29 15 09	2.43	20.6	2004 TL61	MN-MP	<i>g</i>	04:50:57.36	+29:15:10.6	21.45	pho1	
20221026	21:13:28	04 51 40.4	+29 20 13	1.4	21.1	2011 SS235	MNVF	<i>g</i>	04:51:40.30	+29:20:12.5	22.14	pho1	
20221026	21:14:08	04 52 19.9	+29 21 22	2.56	21	2015 BQ42	MNVF	<i>g</i>	04:52:19.80	+29:21:19.8	21.96	pho1	
20221026	21:14:24	04 52 36.4	+29 11 06	0.89	21.4	2015 CP64	MNVF	<i>g</i>	04:52:36.45	+29:11:06.6	21.19	pho1	
20221026	21:15:11	04 53 23.9	+29 09 18	1.01	20.8	2011 UN326	MNVF	<i>g</i>	04:53:23.89	+29:09:19.0	nomag	pho2	ext
20221026	21:15:16	04 53 28.7	+29 26 54	1.32	19.9	2001 TK10	MP	<i>g</i>	04:53:28.78	+29:26:53.2	20.49	pho1	c++
20221026	21:16:12	04 54 24.8	+29 18 48	0.33	20.8	2007 DX78	MN-MP	<i>g</i>	04:54:24.81	+29:18:47.7	20.9	pho2	
20221026	21:17:18	04 55 30.8	+29 16 21	1.16	20.7	2002 JF147	MN-MP	<i>g</i>	04:55:30.88	+29:16:21.5	21.43	pho1	
20221026	21:17:19	04 55 31.5	+29 24 50	0.88	19.4	1999 XB132	MN-MP	<i>g</i>	04:55:31.56	+29:24:49.6	19.7	pho1	
20221026	21:17:27	04 55 39.5	+29 29 38	0.1	20.1	1997 TW23	MN-MP	<i>g</i>	04:55:39.50	+29:29:37.9	20.12	pho1	
20221026	21:17:32	04 55 44.3	+29 24 34	1.34	19.7	2002 CM221	MP	<i>g</i>	04:55:44.40	+29:24:33.7	19.91	pho1	
20221026	21:18:12	04 56 24.4	+29 12 13	1.05	19.5	2001 VP14	MN-MP	<i>g</i>	04:56:24.48	+29:12:13.1	20.54	pho1	
20221026	21:18:12	04 56 24.5	+29 18 23	0.56	21.5	2015 FD78	MNVF	<i>g</i>	04:56:24.46	+29:18:23.2	21.84	pho1	
20221026	21:18:30	04 56 43.0	+29 28 01	0.92	20	2004 TG158	MN-MP	<i>g</i>	04:56:43.07	+29:28:00.9	20.15	pho1	
20221026	21:18:35	04 56 48.2	+29 26 23	0.39	20.9	2010 KX14	MNVF	<i>g</i>	04:56:48.23	+29:26:23.0	21.57	pho1	
20221026	21:18:47	04 56 59.5	+29 18 07	0.48	21.3	2006 DH80	MNVF	<i>g</i>	04:56:59.48	+29:18:07.4	22	pho2	0.1
20221026	21:18:51	04 57 03.4	+29 21 57	0.52	20.4	2001 XK231	MP	<i>g</i>	04:57:03.44	+29:21:57.0	21.14	pho1	
20221026	21:19:03	04 57 15.8	+29 12 59	0.33	21.1	2008 OX22	MN-MP	<i>g</i>	04:57:15.78	+29:12:58.8	22.11	pho1	
20221026	21:20:13	04 58 25.3	+29 22 46	0.48	21.2	2014 NT70	MN	<i>g</i>	04:58:25.32	+29:22:46.4	20.52	pho1	
20221026	21:20:53	04 59 06.5	+29 27 32	0.56	18.6	2002 DN7	MP	<i>g</i>	04:59:06.48	+29:27:32.5	18.92	pho1	
20221026	21:22:05	05 00 18.1	+29 29 14	1.15	20.6	2014 RD50	MN	<i>g</i>	05:00:18.03	29:29:14.70	nomag	pho2	
20221026	21:22:08	05 00 21.7	+29 26 45	0.72	20.8	2002 CW77	MN-MP	<i>g</i>	05:00:21.66	+29:26:45.5	20.92	pho1	
20221026	21:22:34	05 00 47.9	+29 19 19	1.44	21.6	2016 QY110	MNVF	<i>g</i>	05:00:47.80	+29:26:45.6	22.93	pho2	ext
20221026	21:23:14	05 01 27.6	+29 23 28	1.06	19.8	2001 QO36	MP	<i>g</i>	05:01:27.52	+29:26:45.7	20.45	pho1	
20221026	21:24:02	05 02 16.0	+29 25 05	1.94	21.5	2015 JO14	MNVF	<i>g</i>	05:02:15.89	+29:26:45.8	21.7	pho2	
20221026	21:24:03	05 02 17.0	+29 24 13	0.94	20.7	2004 GC42	MP	<i>g</i>	05:02:16.98	+29:26:45.9	21.09	pho1	
20221026	21:24:14	05 02 28.3	+29 13 55	1.68	20.5	2000 SQ115	MN	<i>g</i>	05:02:28.18	+29:26:45.10	20.72	pho2	
20221026	21:24:18	05 02 31.3	+29 24 52	1.84	21.3	2010 AMI66	MNVF	<i>g</i>	05:02:31.43	+29:26:45.11	21.56	pho2	

continued.

<i>Date</i>	<i>Time(UT1)</i>	<i>RA(hms)</i>	<i>Dec(dms)</i>	<i>Dist(″)</i>	<i>Mag(V)</i>	<i>Name</i>	<i>Class</i>	<i>F</i>	<i>RA<sub>det</sub></i>	<i>Dec<sub>det</sub></i>	<i>Mag<sub>det</sub></i>	<i>Flag</i>	<i>Notes</i>
20221026	21:24:28	05 02 42.2	+29 14 26	0.93	21.2	2013 EE66	MNVF	<i>g</i>	05:02:42.14	+29:26:45.12	20.46	pho1	
20221026	21:25:03	05 03 16.7	+29 16 34	1.07	18.6	Melanthios	MP	<i>g</i>	05:03:16.62	+29:26:45.13	19.37	pho1	
20221026	21:25:11	05 03 25.2	+29 23 25	1.57	20.9	2008 SP198	MNVF	<i>g</i>	05:03:25.08	+29:26:45.14	22.08	pho1	
20221026	21:25:32	05 03 45.8	+29 27 07	1.21	20.1	2003 UV192	MIN-MP	<i>g</i>	05:03:45.73	+29:26:45.15	20.68	pho1	
20221026	21:25:42	05 03 55.4	+29 18 47	0.93	19.4	2000 HF12	MP	<i>g</i>	05:03:55.34	+29:26:45.16	19.99	pho1	
20221026	21:25:43	05 03 56.9	+29 27 28	2.3	18	1990 QQ4	MP	<i>g</i>	05:03:56.76	+29:26:45.17	18.43	pho1	
20221026	21:26:14	05 04 28.3	+29 10 21	1.78	21.5	2015 VD27	MNVF	<i>g</i>	05:04:28.26	+29:26:45.18	21.79	pho1	
20221026	21:26:20	05 04 33.6	+29 24 30	6.92	18.8	2001 UB18	MIN	<i>g</i>	05:04:33.70	+29:26:45.19	19.35	pho2 > 4″	
20221027	21:26:21	05 04 35.2	+29 18 43	2.76	22	2002 PV17	MNVF	<i>g</i>	05:04:34.99	+29:26:45.20	21.83	pho2 0.2	
20221027	21:07:59	04 50 07.1	+29 11 19	1.37	21.1	2011 FR	MIN	<i>g</i>	04:50:07.00	+29:26:45.21	21.58	pho2	
20221027	21:08:10	04 50 17.8	+29 27 52	0.52	20.9	2008 CY138	MIN-MP	<i>g</i>	04:50:17.81	+29:26:45.22	21.42	pho1	
20221027	21:08:16	04 50 24.2	+29 19 21	1.59	20.6	2004 TL61	MP	<i>g</i>	04:50:24.10	+29:26:45.23	21.15	pho1	
20221027	21:08:17	04 50 24.7	+29 17 40	2.97	21.5	2003 SW454	MNVF	<i>g</i>	04:50:24.59	+29:26:45.24	20.73	pho1	
20221027	21:09:10	04 51 18.3	+29 18 49	1.47	21.1	2011 SS235	MINF	<i>g</i>	04:51:18.19	+29:26:45.25	22.19	pho1	
20221027	21:09:43	04 51 51.3	+29 13 53	1.65	21	2015 BQ42	MNVF	<i>g</i>	04:51:51.19	+29:26:45.26	21.9	pho1	
20221027	21:09:53	04 52 00.6	+29 22 17	0.26	21.5	2009 SH359	MNVF	<i>g</i>	04:52:00.58	+29:26:45.27	22.11	pho2 ext	
20221027	21:09:55	04 52 03.1	+29 09 16	2	21.7	2012 SD25	MNVF	<i>g</i>	04:52:03.02	+29:26:45.28	21.98	pho2 ext	
20221027	21:09:59	04 52 07.5	+29 12 01	1.32	21.3	2015 CP64	MINF	<i>g</i>	04:52:07.42	+29:26:45.29	21.66	pho1	
20221027	21:10:52	04 53 00.3	+29 20 20	2.25	21.7	2014 YW98	MINF	<i>g</i>	04:53:00.15	+29:26:45.30	21.64	pho2	
20221027	21:11:43	04 53 52.2	+29 19 49	3.64	20.7	2018 RE28	MIN	<i>g</i>	04:53:52.1	+29:26:45.31	21.53	pho2 > 4″	
20221027	21:11:55	04 54 04.2	+29 21 53	0.93	20.8	2007 DX78	MP	<i>g</i>	04:54:04.14	+29:26:45.32	21.05	0.2	
20221027	21:12:10	04 54 19.2	+29 15 51	3.29	21.9	2013 JK15	MNVF	<i>g</i>	04:54:19.0	+29:26:45.33	22.14	pho1	
20221027	21:12:47	04 54 55.8	+29 16 58	2.62	20.7	2002 JF147	MIN	<i>g</i>	04:54:55.6	+29:26:45.34	nomag	pho2 ext ld	
20221027	21:13:00	04 55 09.1	+29 27 01	1.28	19.4	1999 XB132	MP	<i>g</i>	04:55:09.03	+29:26:45.35	19.61	pho2 c++	
20221027	21:13:04	04 55 13.3	+29 27 54	2.32	19.7	2002 CM221	MP	<i>g</i>	04:55:13.14	+29:26:45.36	19.6	pho1	
20221027	21:13:56	04 56 04.7	+29 12 15	2.25	19.5	2001 VP14	MP	<i>g</i>	04:56:04.53	+29:26:45.37	20.37	pho1	
20221027	21:14:03	04 56 11.5	+29 25 26	1.77	21.4	2010 VW257	MNVF	<i>g</i>	04:56:11.37	+29:26:45.38	22.6	pho1	
20221027	21:14:18	04 56 27.0	+29 20 50	2.61	21.4	2015 MX19	MNVF	<i>g</i>	04:56:26.8	+29:26:45.39	21.92	pho2 ext ld	
20221027	21:14:22	04 56 30.6	+29 19 15	3.29	21.3	2006 DH80	MNVF	<i>g</i>	04:56:30.35	+29:26:45.40	21.5	pho2	
20221027	21:14:29	04 56 37.5	+29 21 14	1.44	20.4	2001 XK231	MP	<i>g</i>	04:56:37.60	+29:26:45.41	21.01	pho1	
20221027	21:14:47	04 56 55.9	+29 13 18	1.05	21.1	2008 OX22	MINF	<i>g</i>	04:56:55.98	+29:26:45.42	21.74	pho1	

continued.

<i>Date</i>	<i>Time(UT1)</i>	<i>RA(hms)</i>	<i>Dec(dms)</i>	<i>Dist(″)</i>	<i>Mag(V)</i>	<i>Name</i>	<i>Class</i>	<i>F</i>	<i>RA<sub>det</sub></i>	<i>Dec<sub>det</sub></i>	<i>Mag<sub>det</sub></i>	<i>Flag</i>	<i>Notes</i>
20221027	21:15:41	04 57 49.8	+29 27 10	1.19	22	2010 CZ29	MNVF	<i>g</i>	04:57:49.85	+29:26:45.43	22.48	pho1	
20221027	21:16:00	04 58 09.0	+29 23 13	2.49	21.2	2014 NT70	MNVF	<i>g</i>	04:58:08.81	+29:26:45.44	20.73	pho1	
20221027	21:17:10	04 59 19.1	+29 13 20	1.7	21.3	2001 TS251	MNVF	<i>g</i>	04:59:19.21	+29:26:45.45	21.91	pho1	
20221027	21:17:19	04 59 27.4	+29 15 05	1	21.2	2011 JK10	MNVF	<i>g</i>	04:59:27.4	+29:26:45.46	22.13	pho2	ext
20221027	21:17:31	04 59 40.5	+29 17 49	1	21.5	2008 XL25	MNVF	<i>g</i>	04:59:40.57	+29:26:45.47	21.74	pho1	
20221027	21:17:51	05 00 00.5	+29 28 49	1.09	20.8	2002 CW77	MN-MP	<i>g</i>	05:00:00.58	+29:28:48.7	21.33	pho1	
20221027	21:18:37	05 00 46.3	+29 22 40	0.6	21.5	2009 UZ18	MNVF	<i>g</i>	05:00:46.34	+29:22:39.7	22.21	pho1	
20221027	21:18:51	05 01 00.7	+29 10 42	0.24	20	2011 BJ132	MP	<i>g</i>	05:01:00.69	+29:10:41.8	20.22	pho1	
20221027	21:18:57	05 01 06.9	+29 24 34	0.4	19.8	2001 QO36	MP	<i>g</i>	05:01:06.93	+29:24:33.9	20.36	pho1	
20221027	21:19:40	05 01 49.7	+29 28 17	1.23	21.5	2015 JO14	MNVF	<i>g</i>	05:01:49.68	+29:28:18.2	22.23	pho1	
20221027	21:19:45	05 01 54.3	+29 27 50	0.28	20.6	2004 GC42	MIN	<i>g</i>	05:01:54.28	+29:27:49.9	20.71	pho1	
20221027	21:19:51	05 02 00.6	+29 18 02	0.16	20.5	2000 SQ115	MN-MP	<i>g</i>	05:02:00.61	+29:18:01.9	21.72	pho1	
20221027	21:20:09	05 02 18.5	+29 13 24	0.2	21.2	2013 EE66	MNVF	<i>g</i>	05:02:18.50	+29:13:24.2	22.01	pho1	
20221027	21:20:48	05 02 57.8	+29 17 23	0.28	18.6	Melanthios	MN-MP	<i>g</i>	05:02:57.82	+29:17:22.9	19.32	pho1	
20221027	21:20:56	05 03 05.2	+29 21 34	0.48	21.2	2010 AM166	MN-MP	<i>g</i>	05:03:05.22	+29:21:33.6	22.02	pho1	
20221027	21:20:57	05 03 06.9	+29 23 10	0.2	20.9	2008 SP198	MNVF	<i>g</i>	05:03:06.90	+29:23:09.8	22.06	pho1	
20221027	21:21:18	05 03 27.2	+29 28 24	0.3	20.1	2003 UV192	MP	<i>g</i>	05:03:27.20	+29:28:24.3	19.11:	pho1	c+ hal
20221027	21:21:19	05 03 28.2	+29 23 12	0.56	19.3	2000 HF12	MP	<i>g</i>	05:03:28.16	+29:23:11.8	20.17	pho1	
20221027	21:21:29	05 03 39.1	+29 21 34	0.65	19.4	2001 TN65	MP	<i>g</i>	05:03:39.05	+29:21:34.0	19.72	pho1	
20221027	21:21:35	05 03 45.2	+29 09 46	1.09	21.2	2013 WA78	MP	<i>g</i>	05:03:45.12	+29:09:46.3	21.99	pho1	
20221027	21:21:46	05 03 55.4	+29 19 19	1.65	21.7	2015 FA186	MP	<i>g</i>	05:03:55.3	+29:19:20	nomag	pho3	c++
20221027	21:22:15	05 04 25.2	+29 16 06	0.41	21.5	2015 VD27	MNVF	<i>g</i>	05:04:25.17	+29:16:05.9	22	pho1	
20221028	21:03:29	04 49 33.1	+29 14 57	0.89	21.1	2011 FR	MP	<i>i</i>	04:49:33.15	+29:14:56.4	20.38	pho1	
20221028	21:03:45	04 49 48.5	+29 23 29	1.62	20.6	2004 TL61	MP	<i>i</i>	04:49:48.62	+29:23:28.6	nomag	pho2	c++
20221028	21:03:54	04 49 57.9	+29 16 27	0.66	21.5	2003 SW454	MP	<i>i</i>	04:49:57.94	+29:16:27.4	21.36	pho1	
20221028	21:04:11	04 50 15.0	+29 11 20	0.84	22.4	2007 FK56	MNVF	<i>i</i>	04:50:15.06	+29:11:19.7	22	pho1	
20221028	21:04:12	04 50 15.6	+29 16 14	0.3	22.4	2018 LJ18	MNVF	<i>i</i>	04:50:15.60	+29:16:14.3	21.96	pho1	
20221028	21:04:42	04 50 45.6	+29 23 01	0.44	21	2010 LF53	MP	<i>i</i>	04:50:45.63	+29:23:01.2	20.24	pho1	
20221028	21:04:51	04 50 54.5	+29 17 19	0.41	21.1	2011 SS235	MN-MP	<i>i</i>	04:50:54.53	+29:17:18.9	21.56	pho1	
20221028	21:04:59	04 51 02.8	+29 29 47	0.72	21.9	2017 FK36	MIN	<i>i</i>	04:51:02.84	+29:29:47.5	21.37	pho2	ext
20221028	21:05:14	04 51 17.3	+29 28 16	1.35	21.8	2015 MX6	MNVF	<i>i</i>	04:51:17.37	+29:28:17.0	21.4	pho1	
20221028	21:05:21	04 51 25.2	+29 23 40	1.19	21.4	2009 SH359	MP	<i>i</i>	04:51:25.26	+29:23:39.1	20.87	pho1	

continued.

<i>Date</i>	<i>Time(UT1)</i>	<i>RA(hms)</i>	<i>Dec(dms)</i>	<i>Dist(°)</i>	<i>Mag(V)</i>	<i>Name</i>	<i>Class</i>	<i>F</i>	<i>RA<sub>det</sub></i>	<i>Dec<sub>det</sub></i>	<i>Mag<sub>det</sub></i>	<i>Flag</i>	<i>Notes</i>
20221028	21:05:30	04 51 34.2	+29 11 31	1.11	21.6	2012 SD25	MNVF	<i>i</i>	04:51:34.19	+29:11:32.1	22.09	pho2	2*
20221028	21:06:08	04 52 11.5	+29 26 24	0.4	21.4	2012 TC44	MIN-MP	<i>i</i>	04:52:11.52	+29:26:24.3	21.84	pho1	
20221028	21:06:28	04 52 32.1	+29 23 49	0.16	21.7	2014 YW98	MIN	<i>i</i>	04:52:32.11	+29:23:49.1	21.33	pho1	
20221028	21:07:11	04 53 14.8	+29 12 07	1	21.5	2004 MF9	MP	<i>i</i>	04:53:14.73	+29:12:06.6	20.66	pho1	
20221028	21:07:37	04 53 41.1	+29 24 55	0.78	20.7	2007 DX78	MP	<i>i</i>	04:53:41.04	+29:24:55.0	20.2	pho1	
20221028	21:07:37	04 53 41.5	+29 08 44	1.81	21.8	2009 WG84	MIN-MP	<i>i</i>	04:53:41.39	+29:08:45.1	21.51	pho1	
20221028	21:07:43	04 53 47.0	+29 26 29	1.38	22.5	2021 QQ71	MNVF	<i>i</i>	04:53:46.92	+29:26:29.9	21.98	pho2	prev
20221028	21:08:00	04 54 04.4	+29 12 31	1.43	19.4	2011 AW79	MP	<i>i</i>	04:54:04.33	+29:12:32.1	19.01	pho1	
20221028	21:08:13	04 54 18.1	+29 17 29	1.47	20.7	2002 JF147	MP	<i>i</i>	04:54:17.99	+29:17:28.7	20.2	pho1	
20221028	21:08:40	04 54 45.0	+29 29 10	1.11	19.4	1999 XB132	MP	<i>i</i>	04:54:44.99	+29:29:11.1	18.7	pho1	
20221028	21:09:38	04 55 42.7	+29 12 12	1.22	19.4	2001 VP14	MP	<i>i</i>	04:55:42.61	+29:12:12.3	18.99	pho1	
20221028	21:09:39	04 55 43.7	+29 20 59	0.66	21.5	2015 FD78	MP	<i>i</i>	04:55:43.66	+29:20:59.4	20.99	pho2	prev
20221028	21:09:47	04 55 51.6	+29 25 19	0.66	21.4	2010 VW257	MIN-MP	<i>i</i>	04:55:51.55	+29:25:19.1	21.86	pho1	
20221028	21:09:48	04 55 53.2	+29 21 40	0.64	21.4	2016 TZ33	MIN-MP	<i>i</i>	04:55:53.17	+29:21:39.5	21.38	pho1	
20221028	21:09:51	04 55 55.6	+29 24 47	0.53	20.8	2010 KX14	MP	<i>i</i>	04:55:55.56	+29:24:46.9	20.66	pho1	
20221028	21:09:55	04 55 59.6	+29 20 19	0.96	21.3	2006 DH80	MP	<i>i</i>	04:55:59.53	+29:20:19.3	21	pho1	
20221028	21:09:58	04 56 02.6	+29 23 16	1.21	21.4	2015 MX19	MIN	<i>i</i>	04:56:02.52	+29:23:16.6	21.43	pho1	
20221028	21:10:05	04 56 10.3	+29 20 27	1.45	20.4	2001 XK231	MP	<i>i</i>	04:56:10.19	+29:20:27.2	20.02	pho1	
20221028	21:10:16	04 56 20.9	+29 17 05	1.7	21.6	2010 RP92	MIN-MP	<i>i</i>	04:56:20.77	+29:17:05.1	21.16	pho2	2*
20221028	21:10:30	04 56 35.4	+29 13 35	0.77	21.1	2008 OX22	MP	<i>i</i>	04:56:35.35	+29:13:35.4	20.53	pho1	
20221028	21:11:46	04 57 50.6	+29 23 34	1.57	21.2	2014 NT70	MP	<i>i</i>	04:57:50.48	+29:23:34.1	21.45	pho1	
20221028	21:11:54	04 57 58.8	+29 27 44	0.92	21.6	2019 AG42	MIN	<i>i</i>	04:57:58.73	+29:27:44.1	20.95	pho1	
20221028	21:11:59	04 58 03.8	+29 08 09	2.2	20.2	2005 CV11	MIN-MP	<i>i</i>	04:58:03.67	+29:08:10.4	20.37	pho1	
20221028	21:12:36	04 58 40.2	+29 29 20	1.37	21.7	2015 TQ55	MIN	<i>i</i>	04:58:40.15	+29:29:21.2	20.57	pho1	
20221028	21:12:44	04 58 49.2	+29 19 00	3.48	21.3	2001 TS251	MP	<i>i</i>	04:58:48.96	+29:19:01.5	21.17	pho2	2*
20221028	21:12:49	04 58 53.8	+29 16 50	2.72	21.2	2011 JK10	MP	<i>i</i>	04:58:53.61	+29:16:51.1	20.81	pho1	
20221028	21:13:03	04 59 08.1	+29 20 24	2.2	21.4	2008 XL25	MIN-MP	<i>i</i>	04:59:07.95	+29:20:25.0	21.37	pho1	
20221028	21:13:51	04 59 56.4	+29 16 24	2.23	21.5	2016 QY110	MNBS	<i>i</i>	04:59:56.23	+29:16:23.9	nomag	pho2	c+
20221028	21:13:55	04 59 59.8	+29 18 57	3.56	22	2014 HS7	MNVF	<i>i</i>	04:59:59.88	+29:19:00.4	21.76	pho2	byh prev
20221028	21:14:21	05 00 26.5	+29 24 08	1.04	21.5	2009 UZ18	MIN	<i>i</i>	05:00:26.43	+29:24:08.5	21.16	pho1	uncert

continued.

<i>Date</i>	<i>Time(UT1)</i>	<i>RA(hms)</i>	<i>Dec(dms)</i>	<i>Dist(°)</i>	<i>Mag(V)</i>	<i>Name</i>	<i>Class</i>	<i>F</i>	<i>RA<sub>det</sub></i>	<i>Dec<sub>det</sub></i>	<i>Mag<sub>det</sub></i>	<i>Flag</i>	<i>Notes</i>
20221028	21:14:27	05 00 32.6	+29 16 43	1.16	22.1	2015 BB420	MIN-MP	<i>i</i>	05:00:32.68	+29:16:42.5	22.26	pho1	
20221028	21:14:38	05 00 43.8	+29 25 33	1.57	19.7	2001 QO36	MP	<i>i</i>	05:00:43.92	+29:25:33.1	19.64	pho1	
20221028	21:15:04	05 01 09.4	+29 10 55	0.81	19.9	2011 BJI32	MP	<i>i</i>	05:01:09.34	+29:10:55.2	19.46	pho1	
20221028	21:15:25	05 01 30.7	+29 22 06	1.92	20.4	2000 SQ115	MP	<i>i</i>	05:01:30.83	+29:22:05.1	20.8	pho1	
20221028	21:15:48	05 01 53.4	+29 12 19	0.96	21.2	2013 EE66	MP	<i>i</i>	05:01:53.47	+29:12:19.3	21.2	pho1	
20221028	21:16:21	05 02 26.8	+29 28 45	0.71	21.2	2010 KR90	MIN	<i>i</i>	05:02:26.79	+29:28:44.3	21.6::	pho2	c+
20221028	21:16:32	05 02 38.1	+29 18 10	0.66	18.6	Melanthios	MP	<i>i</i>	05:02:38.14	+29:18:09.6	18.48	pho1	
20221028	21:16:42	05 02 47.8	+29 22 53	0.78	20.9	2008 SP198	MP	<i>i</i>	05:02:47.86	+29:22:53.0	20.565	pho2	
											5		
20221028	21:16:53	05 02 58.9	+29 27 34	1.53	19.3	2000 HF12	MP	<i>i</i>	05:02:59.00	+29:27:33.2	19.09	pho1	
20221028	21:17:01	05 03 06.7	+29 29 37	1.18	20	2003 UV192	MP	<i>i</i>	05:03:06.79	+29:29:37.0	19.58	pho1	
20221028	21:17:06	05 03 11.7	+29 15 44	4.05	21.1	2013 WA78	MP	<i>i</i>	05:03:12	+29:15:45	nomag	pho3	c++
20221028	21:17:11	05 03 16.3	+29 27 23	1.04	19.4	2001 TN65	MP	<i>i</i>	05:03:16.37	+29:27:22.5	18.78:	pho2	uncert prev
20221028	21:17:26	05 03 31.9	+29 16 18	0.56	21.6	2015 FA186	MP	<i>i</i>	05:03:31.92	+29:16:18.5	21.45	pho1	c+
20221028	21:17:30	05 03 36.2	+29 18 02	0.96	21.2	2010 AM166	MIN-MP	<i>i</i>	05:03:36.13	+29:18:02.3	21.06	pho1	byh
20221028	21:17:32	05 03 37.8	+29 18 18	1	22	2002 PV17	MIN-MP	<i>i</i>	05:03:37.87	+29:18:18.4	22.38	pho1	
20221028	21:17:53	05 03 59.1	+29 19 19	0.66	21.2	2005 SB53	MIN-MP	<i>i</i>	05:03:59.15	+29:19:18.9	21.62	pho1	
20221028	21:18:08	05 04 14.0	+29 15 29	0.8	22	2011 YW49	MIN	<i>i</i>	05:04:14.00	+29:15:28.2	22.14	pho1	
20221029	20:59:55	04 49 55.3	+29 20 47	2.77	22.4	2017 SE176	MNVF	<i>i</i>	04:49:55.10	+29:20:46.1	21.6	pho1	
20221029	21:00:16	04 50 15.9	+29 13 55	2.34	20.9	2010 LF53	MP	<i>i</i>	04:50:15.96	+29:13:57.2	20.95	pho1	
20221029	21:00:29	04 50 29.1	+29 15 42	2.08	21.1	2011 SS235	MP	<i>i</i>	04:50:29.23	+29:15:43.2	20.15	pho1	
20221029	21:00:47	04 50 46.4	+29 26 25	2.31	21.8	2015 MX6	MNVF	<i>i</i>	04:50:46.52	+29:26:26.7	21.58	pho2	
20221029	21:00:48	04 50 47.9	+29 24 56	1	21.4	2009 SH359	MNBS	<i>i</i>	04:50:47.97	+29:24:56.4	nomag	pho2	c+
20221029	21:01:04	04 51 04.1	+29 13 37	1.37	21.3	2015 CP64	MP	<i>i</i>	04:51:04.20	+29:13:37.4	21.39	pho1	byh
20221029	21:01:42	04 51 41.8	+29 26 19	1.61	21.4	2012 TC44	MIN-MP	<i>i</i>	04:51:41.89	+29:26:20.1	20.84	pho2	prev
20221029	21:02:02	04 52 01.9	+29 27 13	0.96	21.6	2014 YW98	MNF	<i>i</i>	04:52:01.95	+29:27:12.3	21.68	pho1	
20221029	21:02:46	04 52 46.1	+29 09 24	1.49	21.4	2004 MF9	MP	<i>i</i>	04:52:46.14	+29:09:25.4	21.52	pho1	
20221029	21:03:13	04 53 12.8	+29 09 50	0.8	21.8	2009 WG84	MIN-MP	<i>i</i>	04:53:12.76	+29:09:49.4	22.11	pho1	

continued.

<i>Date</i>	<i>Time(UT1)</i>	<i>RA(hms)</i>	<i>Dec(dms)</i>	<i>Dist(″)</i>	<i>Mag(V)</i>	<i>Name</i>	<i>Class</i>	<i>F</i>	<i>RA<sub>det</sub></i>	<i>Dec<sub>det</sub></i>	<i>Mag<sub>det</sub></i>	<i>Flag</i>	<i>Notes</i>
20221029	21:03:16	04 53 15.5	+29 27 52	0.94	20.7	2007 DX78	MNBS	<i>i</i>	04:53:15.57	+29:27:51.8	nomag	pho2	c+
20221029	21:03:24	04 53 24.0	+29 14 13	0.91	21.9	2013 JK15	MN-MP	<i>i</i>	04:53:24.01	+29:14:13.9	22.17	pho1	byh
20221029	21:03:38	04 53 38.1	+29 17 52	1.12	20.6	2002 JF147	MP	<i>i</i>	04:53:38.18	+29:17:52.4	20.28	pho1	
20221029	21:03:42	04 53 41.8	+29 19 03	0.52	19.4	2011 AW79	MP	<i>i</i>	04:53:41.79	+29:19:02.5	19.1	pho1	
20221029	21:04:41	04 54 41.9	+29 21 28	0.56	22.1	2016 ED307	MNVF	<i>i</i>	04:54:41.88	+29:21:28.5	21.7	pho2	
20221029	21:05:18	04 55 18.7	+29 12 02	1.19	19.4	2001 VP14	MP	<i>i</i>	04:55:18.64	+29:12:02.9	19.12	pho1	
20221029	21:05:21	04 55 22.0	+29 22 14	1.31	21.5	2015 FD78	MP	<i>i</i>	04:55:22.1	+29:22:14	nomag	pho3	c++
20221029	21:05:24	04 55 25.2	+29 20 43	0.16	21.4	2016 TZ33	MP	<i>i</i>	04:55:25.19	+29:20:42.9	21.61	pho1	
20221029	21:05:26	04 55 27.0	+29 21 19	0.77	21.3	2006 DH80	MN-MP	<i>i</i>	04:55:27.05	+29:21:18.6	21.2	pho1	
20221029	21:05:26	04 55 27.1	+29 23 52	0.66	20.8	2010 KX14	MP	<i>i</i>	04:55:27.05	+29:23:51.9	20.95	pho1	
20221029	21:05:30	04 55 30.8	+29 25 09	0.24	21.4	2010 VW257	MP	<i>i</i>	04:55:30.81	+29:25:08.8	21.1	pho1	
20221029	21:05:32	04 55 32.6	+29 21 30	0.93	19.9	2003 VH2	MP	<i>i</i>	04:55:32.66	+29:21:30.5	nomag	pho2	c++
20221029	21:05:36	04 55 36.4	+29 25 38	0.77	21.3	2015 MX19	MP	<i>i</i>	04:55:36.45	+29:25:38.4	21.24	pho1	byh
20221029	21:05:40	04 55 40.8	+29 18 01	0.1	21.2	2010 HR49	MP	<i>i</i>	04:55:40.80	+29:18:00.9	21.77	pho1	
20221029	21:05:41	04 55 41.3	+29 19 35	0.49	20.3	2001 XK231	MP	<i>i</i>	04:55:41.33	+29:19:34.7	nomag	pho2	c++
20221029	21:05:47	04 55 48.1	+29 25 02	0.66	21.5	2014 WP6	MN-MP	<i>i</i>	04:55:48.15	+29:25:01.9	20.83	pho1	byh
20221029	21:05:55	04 55 55.4	+29 15 30	0	21.6	2010 RP92	MN-MP	<i>i</i>	04:55:55.40	+29:15:30.0	22.01	pho1	
20221029	21:06:13	04 56 13.9	+29 13 50	0.66	21	2008 OX22	MP	<i>i</i>	04:56:13.85	+29:13:49.9	20.39	pho1	
20221029	21:06:41	04 56 41.7	+29 17 12	0.44	21.9	2015 VX90	MN-MP	<i>i</i>	04:56:41.67	+29:17:12.2	21.12	pho2	
20221029	21:07:29	04 57 29.7	+29 23 48	1.03	21.1	2014 NT70	MN-MP	<i>i</i>	04:57:29.68	+29:23:49.0	20.39	pho1	
20221029	21:07:31	04 57 32.0	+29 28 14	0.56	21.6	2019 AG42	MNBS	<i>i</i>	04:57:31.97	+29:28:14.4	nomag	pho2	c+
20221029	21:07:45	04 57 45.9	+29 11 36	0.9	20.1	2005 CV11	MP	<i>i</i>	04:57:45.90	+29:11:36.9	19.96	pho1	byh
20221029	21:08:17	04 58 17.7	+29 18 31	0.82	21.2	2011 JK10	MN-MP	<i>i</i>	04:58:17.65	+29:18:31.5	nomag	pho2	c+
20221029	21:08:33	04 58 33.8	+29 22 57	1.65	21.4	2008 XL25	MN-MP	<i>i</i>	04:58:33.7	+29:22:58	nomag	pho3	c++
20221029	21:09:27	04 59 28.3	+29 14 49	1.65	21.5	2016 QY110	MNVF	<i>i</i>	04:59:28.19	+29:14:48.2	22	pho1	
20221029	21:09:28	04 59 29.1	+29 22 32	0.92	22	2014 HS7	MP	<i>i</i>	04:59:29.03	+29:22:32.1	21.83	pho1	
20221029	21:10:05	05 00 05.6	+29 25 35	1.64	21.5	2009 UZ18	MP	<i>i</i>	05:00:05.49	+29:25:35.8	20.94	pho2	

continued.

<i>Date</i>	<i>Time(UT1)</i>	<i>RA(hms)</i>	<i>Dec(dms)</i>	<i>Dist(″)</i>	<i>Mag(V)</i>	<i>Name</i>	<i>Class</i>	<i>F</i>	<i>RA<sub>det</sub></i>	<i>Dec<sub>det</sub></i>	<i>Mag<sub>det</sub></i>	<i>Flag</i>	<i>Notes</i>
20221029	21:10:08	05 00 08.5	+29 18 04	2.36	22.1	2015 BB420	MNVF	<i>i</i>	05:00:08.34	+29:18:05.1	21.53	pho2	
20221029	21:10:18	05 00 18.6	+29 26 25	1.26	19.7	2001 QO36	MP	<i>i</i>	05:00:18.52	+29:26:25.7	19.13	pho1	
20221029	21:10:57	05 00 58.9	+29 26 03	1.69	20.4	2000 SQ115	MP	<i>i</i>	05:00:58.84	+29:26:04.5	19.73	pho1	
20221029	21:11:13	05 01 15.3	+29 11 00	0.68	19.9	2011 BJ132	MP	<i>i</i>	05:01:15.25	+29:11:00.2	19.48	pho1	
20221029	21:11:25	05 01 27.2	+29 11 09	1.96	21.1	2013 EE66	MIN	<i>i</i>	05:01:27.06	+29:11:09.7	20.51	pho1	
20221029	21:12:16	05 02 17.7	+29 18 54	0.81	18.6	Melanthios	MP	<i>i</i>	05:02:17.64	+29:18:54.2	18.5	pho1	
20221029	21:12:26	05 02 28.1	+29 22 33	0.88	20.9	2008 SP198	MP	<i>i</i>	05:02:28.04	+29:22:32.6	20.89	pho1	
20221029	21:12:35	05 02 36.6	+29 21 36	2.77	21.1	2013 WA78	MP	<i>i</i>	05:02:36.40	+29:21:36.9	nomag	pho2	c++
20221029	21:12:50	05 02 50.4	+29 22 52	3.56	21.7	2022 SJ315	MP	<i>i</i>	05:02:50.35	+29:22:55.5	21.17	pho2	byh
20221029	21:13:05	05 03 06.9	+29 13 13	2.8	21.6	2015 FA186	MIN-MP	<i>i</i>	05:03:06.7	+29:13:12	21.39	pho2	
20221029	21:13:05	05 03 07.3	+29 18 00	2.56	22	2002 PV17	MNVF	<i>i</i>	05:03:07.11	+29:18:00.6	21.59	pho1	
20221029	21:13:30	05 03 31.6	+29 20 06	2.52	21.2	2005 SB53	MIN-MP	<i>i</i>	05:03:31.42	+29:20:06.9	21.68	pho1	
20221029	21:13:45	05 03 47.3	+29 20 10	3.5	21.9	2011 YW49	MNVF	<i>i</i>	05:03:47.08	+29:20:12.0	22.14	pho1	
20221029	21:14:02	05 04 04.1	+29 14 19	2.08	21.2	2010 AM166	MP	<i>i</i>	05:04:04.18	+29:14:17.2	21.51	pho1	
20221029	21:14:10	05 04 11.2	+29 27 24	3.09	21.4	2015 VD27	MIN	<i>i</i>	05:04:11.10	+29:27:26.8	21.47	pho2	
20221029	21:14:18	05 04 20.0	+29 25 13	1.12	21.8	2013 AS85	MNVF	<i>i</i>	05:04:19.92	+29:25:13.4	21.82	pho1	
20221030	20:55:46	04 49 41.8	+29 14 11	1.88	22.1	2008 TS76	MNVF	<i>i</i>	04:49:41.66	+29:14:10.6	21.82	pho1	
20221030	20:56:03	04 49 59.2	+29 28 19	1.19	21.8	2017 FK36	MP	<i>i</i>	04:49:59.11	+29:28:18.8	20.28:	pho1	c+
20221030	20:56:06	04 50 02.3	+29 14 01	1.31	21	2011 SS235	MIN-MP	<i>i</i>	04:50:02.2	+29:14:01	nomag	pho3	c++
20221030	20:56:13	04 50 09.0	+29 26 06	2.08	21.4	2009 SH359	MP	<i>i</i>	04:50:08.85	+29:26:06.7	21.94	pho1	
20221030	20:56:19	04 50 14.5	+29 24 30	1.16	21.8	2015 MX6	MIN-MP	<i>i</i>	04:50:14.42	+29:24:29.5	21.6	pho1	
20221030	20:56:19	04 50 14.8	+29 29 22	0.87	20.5	2016 QU77	MP	<i>i</i>	04:50:14.76	+29:29:22.7	20.29	pho1	
20221030	20:56:34	04 50 30.2	+29 14 17	1.84	21.3	2015 CP64	MP	<i>i</i>	04:50:30.07	+29:14:17.7	20.84	pho1	
20221030	20:57:15	04 51 10.9	+29 26 10	2.61	21.4	2012 TC44	MIN-MP	<i>i</i>	04:51:10.70	+29:26:10.0	22.02	pho1	
20221030	20:58:12	04 52 08.0	+29 17 33	2.8	21.6	2010 LZ19	MNVF	<i>i</i>	04:52:07.85	+29:17:35.0	20.77	pho1	
20221030	20:58:46	04 52 42.6	+29 10 49	4.05	21.8	2009 WG84	MINBS	<i>i</i>	04:52:42.3	+29:10:50	nomag	pho2	c++
20221030	20:59:00	04 52 56.4	+29 18 09	2.88	20.6	2002 JF147	MP	<i>i</i>	04:52:56.18	+29:18:08.9	20.19	pho1	uncert
20221030	20:59:21	04 53 17.0	+29 25 28	2.46	19.3	2011 AW79	MP	<i>i</i>	04:53:16.88	+29:25:29.9	19.01	pho1	
20221030	21:00:57	04 54 52.6	+29 11 47	1.44	19.4	2001 VP14	MP	<i>i</i>	04:54:52.71	+29:11:46.9	19.7	pho1	
20221030	21:01:00	04 54 55.8	+29 19 41	1.18	21.4	2016 TZ33	MIN	<i>i</i>	04:54:55.89	+29:19:41.0	21.54	pho1	

continued.

<i>Date</i>	<i>Time(UT1)</i>	<i>RA(hms)</i>	<i>Dec(dms)</i>	<i>Dist(")</i>	<i>Mag(V)</i>	<i>Name</i>	<i>Class</i>	<i>F</i>	<i>RA<sub>det</sub></i>	<i>Dec<sub>det</sub></i>	<i>Mag<sub>det</sub></i>	<i>Flag</i>	<i>Notes</i>
20221030	21:01:01	04 54 57.1	+29 22 51	1.38	20.8	2010 KX14	MP	<i>i</i>	04:54:57.18	+29:22:51.9	20.29	pho1	
20221030	21:01:13	04 55 08.5	+29 27 56	1.32	21.3	2015 MX19	MP	<i>i</i>	04:55:08.59	+29:27:56.6	21.31	pho1	
20221030	21:01:13	04 55 09.2	+29 24 56	0.4	21.4	2010 VW257	MP	<i>i</i>	04:55:09.20	+29:24:56.4	21.1	pho2	0.2
20221030	21:01:15	04 55 10.9	+29 18 37	1	20.3	2001 XK231	MP	<i>i</i>	04:55:10.97	+29:18:37.4	19.99	pho1	
20221030	21:01:25	04 55 21.9	+29 12 07	1.7	21.2	2011 US435	MP	<i>i</i>	04:55:22.01	+29:12:06.1	21.44	pho1	
20221030	21:01:32	04 55 28.5	+29 13 49	0.4	21.5	2010 RP92	MP	<i>i</i>	04:55:28.48	+29:13:49.3	21.94	pho1	
20221030	21:01:42	04 55 38.4	+29 26 02	1.64	21.6	2010 MD2	MP	<i>i</i>	04:55:38.51	+29:26:02.8	21.27	pho1	
20221030	21:01:55	04 55 51.5	+29 14 02	1.19	21	2008 OX22	MN-MP	<i>i</i>	04:55:51.59	+29:14:01.8	20.73	pho1	
20221030	21:02:15	04 56 11.8	+29 19 17	0.68	21.9	2015 VX90	MP	<i>i</i>	04:56:11.85	+29:19:17.2	21.55	pho2	
20221030	21:03:07	04 57 03.3	+29 28 40	1.21	21.6	2019 AG42	MN	<i>i</i>	04:57:03.37	+29:28:40.8	21.7	pho1	
20221030	21:03:10	04 57 06.6	+29 23 56	0.33	21.1	2014 NT70	MP	<i>i</i>	04:57:06.62	+29:23:56.2	21.33	pho1	
20221030	21:03:29	04 57 25.8	+29 15 00	0.68	20.1	2005 CV11	MP	<i>i</i>	04:57:25.85	+29:14:59.8	20.08	pho1	
20221030	21:03:43	04 57 39.6	+29 20 07	0.44	21.2	2011 JK10	MN-MP	<i>i</i>	04:57:39.63	+29:20:06.8	21.44	pho1	
20221030	21:03:45	04 57 41.8	+29 30 13	0.6	21.3	2001 TS251	MN	<i>i</i>	04:57:41.84	+29:30:13.3	20.64	pho1	
20221030	21:04:01	04 57 57.8	+29 25 26	0.93	21.4	2008 XL25	MN-MP	<i>i</i>	04:57:57.86	+29:25:26.5	21.95	pho1	
20221030	21:04:23	04 58 19.6	+29 29 56	1.04	16.5	Karbyshhev	MP	<i>i</i>	04:58:19.67	+29:29:56.5	16.16	pho1	
20221030	21:04:31	04 58 27.5	+29 12 54	0.88	22.3	2014 JF71	MNVF	<i>i</i>	04:58:27.44	+29:12:54.4	22	pho2	ext
20221030	21:05:00	04 58 56.9	+29 26 04	0.61	21.9	2014 HS7	MNF	<i>i</i>	04:58:56.89	+29:26:03.4	21	pho2	hal
20221030	21:05:02	04 58 58.7	+29 13 08	0.72	21.5	2016 QY110	MP	<i>i</i>	04:58:58.65	+29:13:08.3	21.6	pho1	
20221030	21:05:46	04 59 42.3	+29 19 22	0.28	22	2015 BB420	MNVF	<i>i</i>	04:59:42.28	+29:19:21.9	21.74	pho2	ext
20221030	21:05:47	04 59 43.3	+29 14 30	0.33	21.1	2008 UX215	MP	<i>i</i>	04:59:43.28	+29:14:29.8	21.12	pho1	0.2
20221030	21:05:47	04 59 43.7	+29 27 00	0.61	21.5	2009 UZ18	MN-MP	<i>i</i>	04:59:43.71	+29:26:59.4	21.44	pho1	
20221030	21:05:54	04 59 50.7	+29 27 11	0.56	19.7	2001 QO36	MP	<i>i</i>	04:59:50.73	+29:27:11.4	19.83	pho1	
20221030	21:06:04	05 00 01.1	+29 10 02	0.42	20.2	2008 FZ69	MP	<i>i</i>	05:00:01.09	+29:10:02.4	20.55	pho1	
20221030	21:06:28	05 00 24.7	+29 29 59	0.52	20.4	2000 SQ115	MP	<i>i</i>	05:00:24.69	+29:29:59.5	20.1	pho1	
20221030	21:06:50	05 00 46.3	+29 11 07	1.87	22.3	2015 BE609	MNVF	<i>i</i>	05:00:46.36	+29:11:05.3	22.27	pho1	
20221030	21:07:02	05 00 59.3	+29 09 55	0.56	21.1	2013 EE66	MP	<i>i</i>	05:00:59.27	+29:09:55.4	21.05	pho1	
20221030	21:07:22	05 01 18.4	+29 10 56	0.64	19.9	2011 BJ132	MP	<i>i</i>	05:01:18.37	+29:10:56.5	19.95	pho1	
20221030	21:07:34	05 01 31.6	+29 23 16	0.39	21.2	2010 KR90	MN-MP	<i>i</i>	05:01:31.57	+29:23:16.0	20.92	pho1	
20221030	21:07:59	05 01 56.3	+29 19 37	0.44	18.6	Melanthios	MP	<i>i</i>	05:01:56.27	+29:19:36.8	18.32	pho1	
20221030	21:08:02	05 01 59.2	+29 27 28	1.53	21.1	2013 WA78	MP	<i>i</i>	05:01:59.10	+29:27:28.8	nomag	pho2	c++

continued.

<i>Date</i>	<i>Time(UT1)</i>	<i>RA(hms)</i>	<i>Dec(dms)</i>	<i>Dist(″)</i>	<i>Mag(V)</i>	<i>Name</i>	<i>Class</i>	<i>F</i>	<i>RA<sub>det</sub></i>	<i>Dec<sub>det</sub></i>	<i>Mag<sub>det</sub></i>	<i>Flag</i>	<i>Notes</i>
20221030	21:08:12	05 02 10.1	+29 16 06	1.65	21.9	2007 VT58	MNVF	<i>i</i>	05:02:10	+29:16:07	nomag	pho2	ext c++
20221030	21:08:37	05 02 34.9	+29 17 38	0.8	22	2002 PV17	MIN-MP	<i>i</i>	05:02:34.86	+29:17:37.4	21.84	pho1	byh
20221030	21:08:42	05 02 39.8	+29 09 58	1.09	21.6	2015 FA186	MIN-MP	<i>i</i>	05:02:39.72	+29:09:58.3	21.40:	pho2	c
20221030	21:09:05	05 03 02.3	+29 20 50	0.68	21.2	2005 SB53	MP	<i>i</i>	05:03:02.25	+29:20:50.2	20.81	pho1	
20221030	21:09:05	05 03 02.8	+29 12 58	2.89	22.3	2006 TD133	MIN	<i>i</i>	05:03:02.69	+29:13:00.5	nomag	pho1	hal
20221030	21:09:20	05 03 18.0	+29 24 51	1.45	21.9	2011 YW49	MNVF	<i>i</i>	05:03:17.92	+29:24:52.0	21.3	pho1	uncert
20221030	21:09:57	05 03 54.6	+29 26 11	1.31	21.7	2013 AS85	MP	<i>i</i>	05:03:54.5	+29:26:11	nomag	pho3	c++
20221030	21:10:23	05 04 21.0	+29 13 31	1.32	16.9	Thorium	MP	<i>i</i>	05:04:20.90	+29:13:30.8	16.6	pho1	
20221030	21:10:32	05 04 29.3	+29 10 19	0	21.1	2010 AM166	MP	<i>i</i>	05:4:29.3	+29:10:19	nomag	pho3	c++
20221031	20:51:33	04 49 24.0	+29 27 24	5.72	21.8	2017 FK36	MNVF	<i>g</i>	04:49:23.57	+29:27:22.9	21.99	pho1	uncert
20221031	20:51:37	04 49 27.8	+29 27 11	0.33	21.4	2009 SH359	MNF	<i>g</i>	04:49:27.81	+29:27:10.7	21.54	pho1	
20221031	20:51:43	04 49 33.7	+29 12 13	1.22	21	2011 SS235	MNVF	<i>g</i>	04:49:33.74	+29:12:14.1	21.81	pho2	
20221031	20:51:50	04 49 41.1	+29 22 28	1.75	21.8	2015 MX6	MNVF	<i>g</i>	04:49:41.01	+29:22:29.3	21.4	pho2	
20221031	20:51:53	04 49 43.6	+29 27 21	0.9	20.5	2016 QU77	MP	<i>g</i>	04:49:43.60	+29:27:21.9	20.74	pho1	
20221031	20:52:02	04 49 54.3	+29 14 52	0.66	21.3	2015 CP64	MNVF	<i>g</i>	04:49:54.34	+29:14:52.4	21.74	pho1	
20221031	20:52:06	04 49 57.8	+29 17 51	0.53	21.6	2012 SD25	MIN-MP	<i>g</i>	04:49:57.76	+29:17:51.1	21.27	pho2	
20221031	20:52:46	04 50 38.0	+29 25 55	0.53	21.4	2012 TC44	MNVF	<i>g</i>	04:50:37.96	+29:25:55.1	21.31	pho2	0.3
20221031	20:54:10	04 52 02.1	+29 07 47	1.43	20.4	2001 QG5	MIN	<i>g</i>	04:52:02.03	+29:07:48.1	21.29	pho1	
20221031	20:54:20	04 52 12.1	+29 18 18	1.19	20.6	2002 JF147	MP	<i>g</i>	04:52:12.01	+29:18:18.2	21.13	pho1	
20221031	20:56:25	04 54 17.3	+29 23 03	1.44	21.3	2006 DH80	MNVF	<i>g</i>	04:54:17.20	+29:23:03.6	21.33	pho2	0.1 2* ext
20221031	20:56:33	04 54 24.9	+29 11 25	1.57	19.4	2001 VP14	MP	<i>g</i>	04:54:24.78	+29:11:24.9	19.81	pho1	
20221031	20:56:33	04 54 25.3	+29 18 35	1.07	21.4	2016 TZ33	MNVF	<i>g</i>	04:54:25.22	+29:18:35.2	22.14	pho1	
20221031	20:56:34	04 54 26.0	+29 21 47	1.83	20.8	2010 KX14	MP	<i>g</i>	04:54:25.86	+29:21:46.9	21.27	pho1	
20221031	20:56:44	04 54 36.5	+29 10 58	1.71	19.9	2000 UU1	MP	<i>g</i>	04:54:36.40	+29:10:59.1	19.67:	pho1	c
20221031	20:56:47	04 54 39.1	+29 30 09	2.04	21.3	2015 MX19	MNF	<i>g</i>	04:54:38.96	+29:30:09.9	21.72	pho1	
20221031	20:56:47	04 54 39.3	+29 17 35	2.02	20.3	2001 XK231	MP	<i>g</i>	04:54:39.15	+29:17:34.5	21.29	pho1	
20221031	20:56:55	04 54 46.9	+29 24 40	2.49	21.4	2010 VW257	MNVF	<i>g</i>	04:54:46.71	+29:24:40.2	21.69	pho1	



continued.

<i>Date</i>	<i>Time(UT1)</i>	<i>RA(hms)</i>	<i>Dec(dms)</i>	<i>Dist(°)</i>	<i>Mag(V)</i>	<i>Name</i>	<i>Class</i>	<i>F</i>	<i>RA<sub>det</sub></i>	<i>Dec<sub>det</sub></i>	<i>Mag<sub>det</sub></i>	<i>Flag</i>	<i>Notes</i>
20221101	20:49:20	04 51 07.5	+29 08 36	1.17	22.6	2001 DY114	MNVF	<i>r</i>	04:51:07.53	+29:08:37.1	21.69	pho2	ext
20221101	20:49:33	04 51 20.7	+29 08 29	0.24	20.4	2001 QG5	MP	<i>r</i>	04:51:20.71	+29:08:28.8	19.41	pho1	0.1
20221101	20:49:38	04 51 25.6	+29 18 20	1.18	20.6	2002 JF147	MP	<i>r</i>	04:51:25.69	+29:18:20.1	20.35	pho1	
20221101	20:49:48	04 51 36.2	+29 12 34	0.28	21.7	2009 WG84	MP	<i>r</i>	04:51:36.18	+29:12:33.9	21.3	pho1	
20221101	20:50:03	04 51 51.5	+29 11 13	1.65	21.8	2013 JK15	MNVF	<i>r</i>	04:51:51.4	+29:11:14	21.6	pho2	ext ld
20221101	20:50:58	04 52 46.0	+29 30 06	0.7	18.7	2001 QC137	MP	<i>r</i>	04:52:46.00	+29:30:06.7	19.05	pho1	
20221101	20:51:52	04 53 39.9	+29 23 48	0.64	21.2	2006 DH80	MP	<i>r</i>	04:53:39.93	+29:23:47.5	21.27	pho1	
20221101	20:52:05	04 53 53.2	+29 20 37	0.75	20.8	2010 KX14	MN-MP	<i>r</i>	04:53:53.18	+29:20:36.3	21.91:	pho1	hal
20221101	20:52:05	04 53 53.3	+29 17 24	0.99	21.4	2016 TZ33	MN-MP	<i>r</i>	04:53:53.24	+29:17:23.4	21.1	pho1	
20221101	20:52:07	04 53 54.9	+29 10 56	0.33	19.3	2001 VP14	MP	<i>r</i>	04:53:54.91	+29:10:56.3	19.4	pho1	
20221101	20:52:10	04 53 57.4	+29 15 29	0.4	19.9	2000 UU1	MP	<i>r</i>	04:53:57.40	+29:15:29.4	19.65	pho1	
20221101	20:52:18	04 54 06.0	+29 16 27	0.81	20.3	2001 XK231	MP	<i>r</i>	04:54:05.94	+29:16:27.2	19.8	pho1	
20221101	20:52:24	04 54 12.2	+29 25 45	0.6	21.5	2015 FD78	MNVF	<i>r</i>	04:54:12.20	+29:25:45.6	22.3	pho1	
20221101	20:52:30	04 54 17.4	+29 21 11	0.8	21.1	2011 US435	MP	<i>r</i>	04:54:17.37	+29:21:11.7	20.71	pho1	
20221101	20:52:37	04 54 24.7	+29 16 10	0	21.6	2010 MD2	MP	<i>r</i>	04:54:24.7	+29:16:10	nomag	pho3	c++
20221101	20:52:42	04 54 30.3	+29 10 12	0.33	21.5	2010 RP92	MP	<i>r</i>	04:54:30.29	+29:10:12.3	21.92	pho1	
20221101	20:53:17	04 55 04.7	+29 14 18	1.18	21	2008 OX22	MP	<i>r</i>	04:55:04.61	+29:14:18.0	20.95	pho1	
20221101	20:53:17	04 55 05.0	+29 08 21	0.6	21.2	2006 DN145	MP	<i>r</i>	04:55:04.96	+29:08:21.3	21.02	pho1	
20221101	20:53:18	04 55 05.7	+29 23 10	1.4	21.8	2015 VX90	MN-MP	<i>r</i>	04:55:05.66	+29:23:11.3	21.7	pho1	
20221101	20:54:06	04 55 54.4	+29 15 19	2.32	21.3	2014 HW257	MP	<i>r</i>	04:55:54.24	+29:15:20.0	21.43	pho2	
20221101	20:54:09	04 55 56.5	+29 18 14	1.83	21.2	2019 TX35	MNVF	<i>r</i>	04:55:56.42	+29:18:15.5	21.78	pho2	prev ext
20221101	20:54:14	04 56 01.2	+29 29 15	0.49	21.5	2019 AG42	MNVF	<i>r</i>	04:56:01.17	+29:29:15.3	nomag	pho2	c+
20221101	20:54:26	04 56 13.9	+29 23 52	1.09	21.1	2014 NT70	MP	<i>r</i>	04:56:13.83	+29:23:51.4	20.74	pho1	
20221101	20:54:30	04 56 17.5	+29 23 00	1.58	21.1	2011 JK10	MP	<i>r</i>	04:56:17.38	+29:23:00.2	20.99	pho1	
20221101	20:54:50	04 56 39.0	+29 21 33	1.21	20	2005 CV11	MP	<i>r</i>	04:56:38.91	+29:21:33.3	20.04	pho1	
20221101	20:54:53	04 56 41.3	+29 30 10	1.33	21.4	2008 XL25	MP	<i>r</i>	04:56:41.28	+29:30:11.3	21.57	pho1	
20221101	20:54:54	04 56 42.9	+29 28 30	0.66	21.3	2013 AS4	MP	<i>r</i>	04:56:42.85	+29:28:29.9	20.99	pho1	
20221101	20:55:12	04 57 00.8	+29 19 30	2.89	22.3	2014 JF71	MP	<i>r</i>	04:57:00.59	+29:19:30.9	21.89	pho2	
20221101	20:55:17	04 57 05.2	+29 28 07	0.53	16.4	Karbyshv	MP	<i>r</i>	04:57:05.16	+29:28:07.1	16.28	pho1	
20221101	20:55:25	04 57 13.4	+29 19 23	1.91	22.3	2016 UR286	MNVF	<i>r</i>	04:57:13.31	+29:19:24.5	21.80	pho2	prev

continued.

<i>Date</i>	<i>Time(UT1)</i>	<i>RA(hms)</i>	<i>Dec(dms)</i>	<i>Dist(″)</i>	<i>Mag(V)</i>	<i>Name</i>	<i>Class</i>	<i>F</i>	<i>RA<sub>det</sub></i>	<i>Dec<sub>det</sub></i>	<i>Mag<sub>det</sub></i>	<i>Flag</i>	<i>Notes</i>
20221101	20:55:34	04 57 23.0	+29 27 37	0.4	19.3	2005 WC161	MP	r	04:57:22.98	+29:27:37.3	19.1	pho1	
20221101	20:56:06	04 57 55.4	+29 09 33	1.48	21.5	2016 QY110	MP	r	04:57:55.31	+29:09:32.1	21.32	pho1	
20221101	20:56:52	04 58 41.2	+29 19 24	2.72	20.2	2008 FZ69	MP	r	04:58:41.01	+29:19:25.1	20.66	pho1	
20221101	20:56:56	04 58 44.7	+29 21 42	1.71	22	2015 BB420	MNVF	r	04:58:44.57	+29:21:42.2	21.61	pho2	
20221101	20:57:00	04 58 48.3	+29 28 21	1.48	19.7	2001 QO36	MN-MP	r	04:58:48.21	+29:28:21.9	19.54	pho1	
20221101	20:57:09	04 58 57.6	+29 29 41	1.09	21.5	2009 UZ18	MN	r	04:58:57.53	+29:29:41.6	21.65	pho1	
20221101	20:57:16	04 59 04.4	+29 08 10	2.43	21.8	2007 HK101	MNVF	r	04:59:04.34	+29:08:07.7	21.05	pho2	prev
20221101	20:57:42	04 59 30.8	+29 10 34	2.65	20.2	2010 TH167	MP	r	04:59:30.61	+29:10:34.9	nomag	pho2	c++
20221101	20:58:42	05 00 30.6	+29 17 25	2.08	21.1	2010 KR90	MP	r	05:00:30.45	+29:17:24.3	20.62:	pho1	c
20221101	20:59:22	05 01 11.2	+29 20 54	1.68	18.6	Melanthios	MN-MP	r	05:01:11.08	+29:20:54.6	18.56	pho1	
20221101	20:59:23	05 01 11.3	+29 28 02	3.36	21.8	2007 VT58	MNVF	r	05:01:11.17	+29:28:04.9	21.97	pho1	
20221101	20:59:28	05 01 16.4	+29 10 23	0.3	19.8	2011 BJ132	MP	r	05:01:16.40	+29:10:22.7	20.57	pho1	
20221101	20:59:35	05 01 23.9	+29 21 18	2.09	20.9	2008 SP198	MP	r	05:01:23.74	+29:21:17.9	20.48	pho1	
20221101	20:59:52	05 01 40.7	+29 27 16	2.49	21.7	2015 MF84	MN-MP	r	05:01:40.51	+29:27:15.8	21.26	pho1	
20221101	21:00:11	05 01 59.6	+29 22 06	0.92	21.2	2005 SB53	MP	r	05:01:59.67	+29:22:06.0	nomag	pho2	c+
20221101	21:00:27	05 02 15.6	+29 08 33	1.04	20.8	2012 TD174	MNVF	r	05:02:15.67	+29:08:33.5	21.54	pho1	
20221101	21:01:07	05 02 56.5	+29 18 49	1.42	21.7	2007 VQ161	MNVF	r	05:02:56.59	+29:18:48.2	22.03	pho2	
20221101	21:01:08	05 02 57.2	+29 27 51	2.64	21.7	2013 AS85	MP	r	05:02:57.40	+29:27:50.6	nomag	pho3	c++
20221101	21:02:21	05 04 10.9	+29 24 11	1.84	18.9	1999 RE208	MP	r	05:04:11.03	+29:24:11.7	18.82	pho1	
20221101	21:02:26	05 04 15.7	+29 25 18	0.84	21.1	2017 FP94	MP	r	05:04:15.76	+29:25:18.3	21.25	pho2	0.1

Table C.2: List of all MPC detections in Field 1317.

<i>Date</i>	<i>Time(UT1)</i>	<i>RA(hms)</i>	<i>Dec(dms)</i>	<i>Dist('')</i>	<i>Mag(V)</i>	<i>Name</i>	<i>Class</i>	<i>F</i>	<i>RA<sub>MPC</sub></i>	<i>Dec<sub>MPC</sub></i>	<i>Mag<sub>det</sub></i>	<i>Flag</i>
20240217	22:21:30	13:28:42.0	+29:30:58	2.39	20.8	2000 WR124	MP	<i>i'</i>	13:28:41.9	+29:31:00	19.80	pho2
20240217	22:24:26	13:31:39.2	+29:34:12	2.39	19.7	2002 JJ58	MP	<i>i'</i>	13:31:39.1	+29:34:14	19.14	pho2
20240217	22:26:15	13:33:29.1	+29:37:15	4.21	19.6	1999 PM1	MN	<i>i'</i>	13:33:29.0	+29:37:19	18.97	pho2
20240217	22:29:22	13:36:37.0	+29:29:39	3.00	19.2	2000 FK1	MP	<i>i'</i>	13:36:37.0	+29:29:36	19.23	pho2
20240217	22:30:44	13:37:59.1	+29:19:04	0.00	21.4	2014 WF498	MNF	<i>i'</i>	13:37:59.1	+29:19:04	20.51	pho2
20240217	22:32:17	13:39:32.0	+29:36:14	0.00	19.6	2002 FM6	MP	<i>i'</i>	13:39:32.0	+29:36:14	19.18	pho2
20240217	22:39:19	13:46:35.0	+29:35:48	6.54	19.8	2006 CV56	MP	<i>i'</i>	13:46:35.2	+29:35:54	19.74	pho2
20240217	23:29:18	14:36:46.9	+29:29:21	0.00	20.8	2009 XS3	MP	<i>i'</i>	14:36:46.9	+29:29:21	20.31	pho2
20240331	19:57:20	13:53:42.7	+29:39:39	1.64	19.1	Martinphillips	MP	<i>r'</i>	13:53:42.6	+29:39:41	18.78	pho2
20240331	20:09:01	14:05:26.3	+29:36:27	1.00	19.4	2012 BJ24	MP	<i>r'</i>	14:05:26.3	+29:36:28	19.33	pho2
20240331	20:20:32	14:16:58.9	+29:36:55	1.64	19.6	2000 WD151	MP	<i>r'</i>	14:16:59.0	+29:36:54	19.66	pho2
20240405	19:48:37	14:04:40.6	+29:21:50	4.78	20.5	2002 QB80	MP	<i>r'</i>	14:04:40.8	+29:21:46	19.64	pho2
20240405	19:53:54	14:09:58.8	+29:35:41	0.00	19.5	2000 WD151	MP	<i>r'</i>	14:09:58.8	+29:35:41	19.25	pho2
20240405	19:58:24	14:14:29.8	+29:23:17	2.39	20.8	2013 CT129	MN	<i>r'</i>	14:14:29.7	+29:23:19	21.76	pho2
20240406	19:48:28	14:08:28.1	+29:22:18	3.27	19.6	2003 FC42	MP	<i>i'</i>	14:08:28.2	+29:22:15	19.12	pho2
20240406	19:48:30	14:08:30.4	+29:33:53	4.04	19.5	2000 WD151	MP	<i>i'</i>	14:08:30.7	+29:33:54	18.97	pho2
20240406	19:53:47	14:13:49.3	+29:30:57	1.00	20.8	2013 CT129	MN	<i>i'</i>	14:13:49.3	+29:30:56	19.87	pho2
20240406	19:58:11	14:18:14.8	+29:35:47	3.29	21.6	2007 AS12	MN	<i>i'</i>	14:18:14.6	+29:35:49	20.67	pho2
20240407	19:43:06	14:07:01.8	+29:31:34	3.92	19.5	2000 WD151	MP	<i>i'</i>	14:07:01.5	+29:31:34	19.45	pho2
20240407	19:43:48	14:07:43.4	+29:34:33	2.39	19.6	2003 FC42	MP	<i>i'</i>	14:07:43.3	+29:34:35	19.09	pho2
20240407	19:49:11	14:13:08.0	+29:38:20	1.64	20.8	2013 CT129	MN	<i>i'</i>	14:13:08.1	+29:38:19	19.77	pho2
20240410	19:38:49	14:14:34.9	+29:18:27	0.00	18.8	1998 QB3	MP	<i>r'</i>	14:14:34.9	+29:18:27	18.53	pho2
20240411	19:34:10	14:13:51.4	+29:29:54	2.39	18.8	1998 QB3	MP	<i>r'</i>	14:13:51.5	+29:29:52	18.73	pho2
20240411	19:38:52	14:18:35.6	+29:21:31	1.00	19.5	2005 YN155	MP	<i>r'</i>	14:18:35.6	+29:21:30	19.19	pho2
20240416	18:57:35	13:56:52.3	+29:34:53	1.00	21.1	2003 AB83	MNVF	<i>i'</i>	13:56:52.3	+29:34:52	19.72	pho2
20240416	19:10:15	14:09:34.1	+29:23:17	0.00	19.8	2004 NL16	MP	<i>i'</i>	14:09:34.1	+29:23:17	19.09	pho2
20240416	19:14:59	14:14:19.9	+29:32:51	1.30	19.5	2005 YN155	MP	<i>i'</i>	14:14:19.8	+29:32:51	18.72	pho2
20240504	18:22:20	14:32:30.7	+29:34:44	2.61	18.0	2001 CE34	MP	<i>r'</i>	14:32:30.9	+29:34:44	17.83	pho2
20240512	17:53:18	14:34:57.1	+29:38:37	3.29	17.1	Hickson	MP	<i>r'</i>	14:34:57.3	+29:38:39	15.86	pho2
20240516	17:31:26	14:28:47.9	+29:25:02	1.31	18.9	1999 YH9	MP	<i>i'</i>	14:28:47.8	+29:25:02	17.96	pho2

**Appendix D Illustration of asteroid classes and notes**

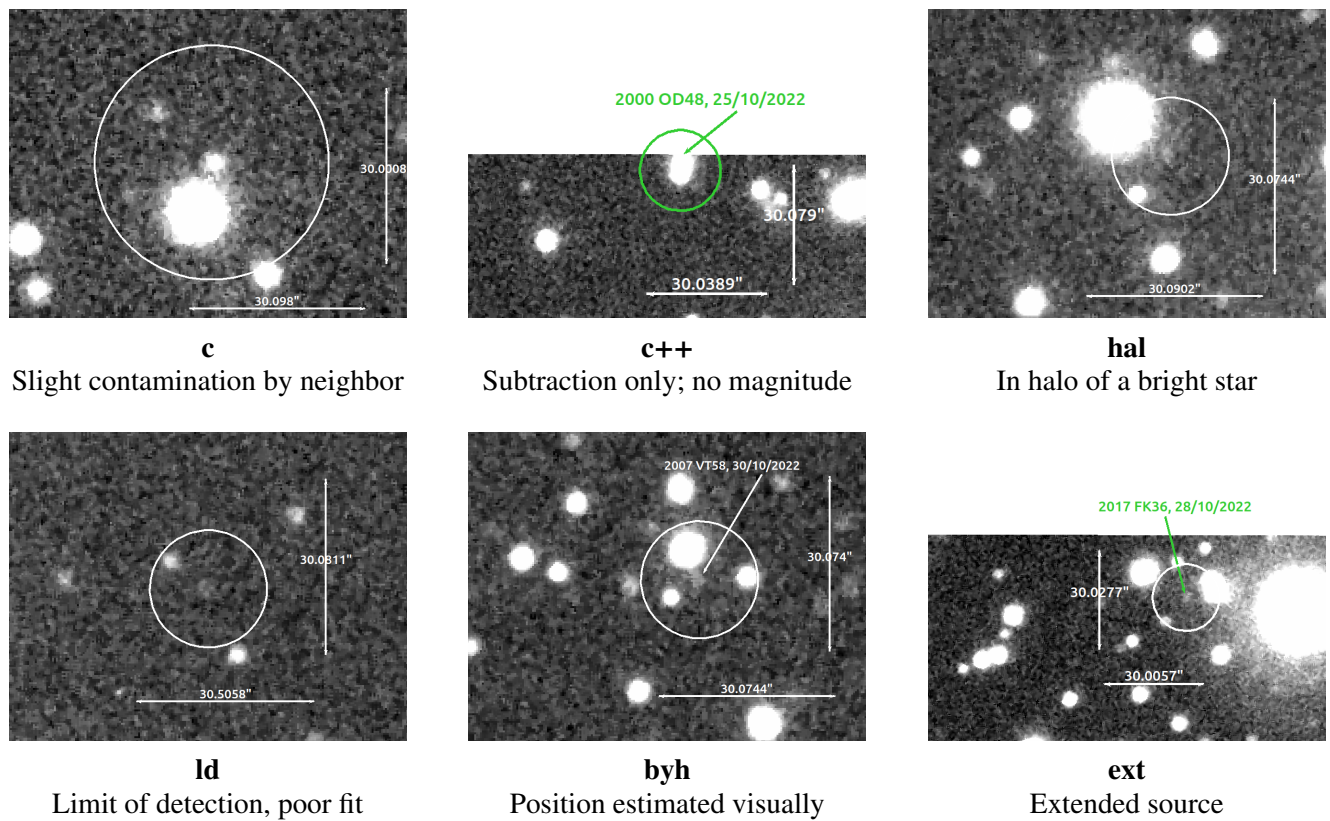


**Figure 12:** Representative zoomed-in cutouts for objects flagged with specific notes. These include cases of contamination, morphology, or difficulty in measurement. Labels refer to: **c** — slight contamination; **c++** — detected only in subtraction; **hal** — in halo of bright star; **ld** — near limit of detection; **byh** — position visually estimated; **ext** — extended morphology. North is up and East is to the left.

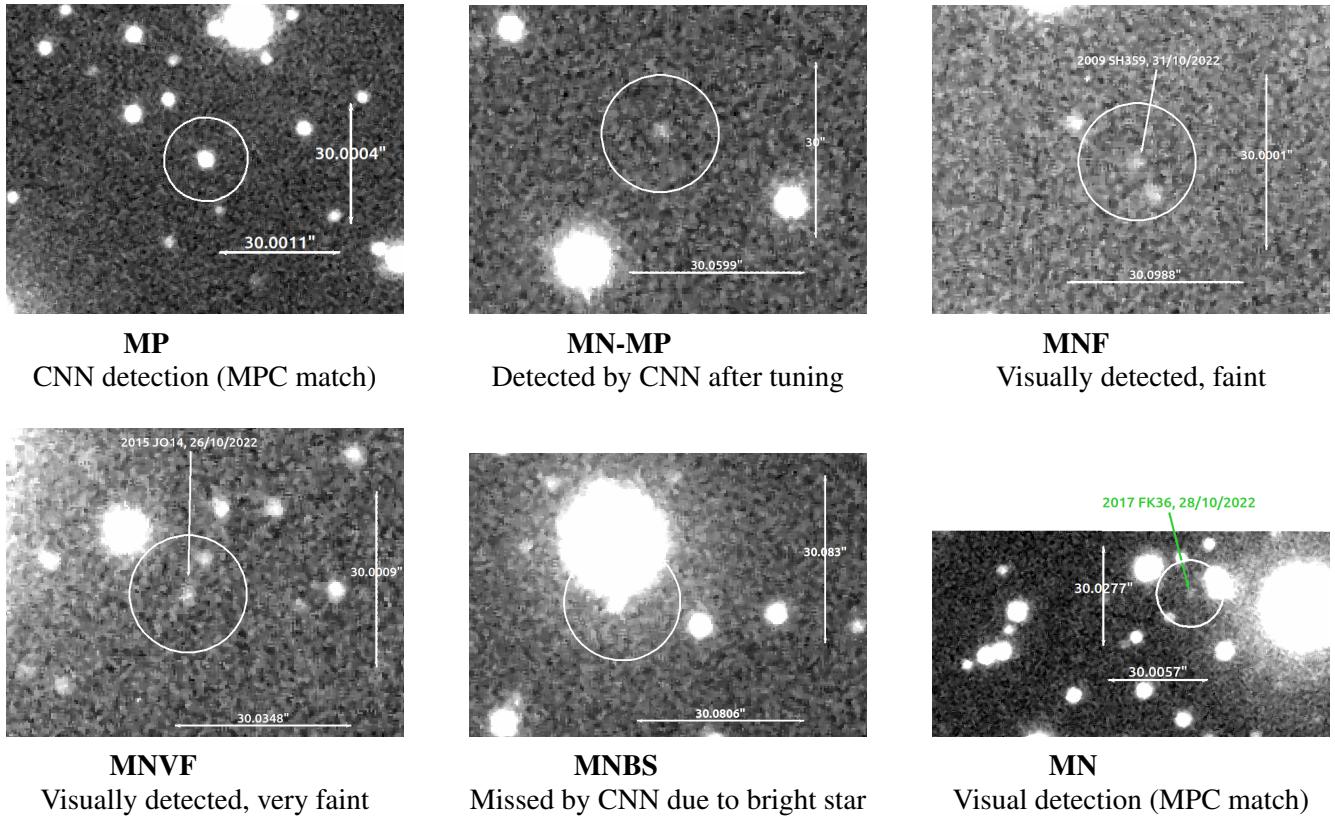


**Figure 13:** Zoomed-in cutouts of representative asteroids for each classification. The circle markers indicate asteroid positions. North is up and East is to the left.

### Appendix E Explanation of the ‘Notes’ column of Table 2

- c: Slight contamination due to a neighbour star; an estimated value for the magnitude is given.
- c+: Due to contamination from a neighbouring star, the magnitude could not be calculated with sufficient precision.
- c++: Detected by subtraction, magnitude cannot be calculated.
- hal: Target is in the halo of a very bright star.
- ld: Limit of detection, detected visually, a gaussian profile does not fit perfectly.
- prev: The same reference stars were used as for the previous target.
- 2\*: No more than two stars were used as references for the zero point calculation.
- byh: The position was estimated visually due to noise or due to a poor gaussian fit.
- ext: The source appears extended, uncertainty on position might follow ( $\sim 1''$ ).
- 2ob: The target appears like two objects instead of one. But it is uncertain due to noise.
- nomag: A magnitude value is not available.
- uncert: Detection considered uncertain or requiring further investigation due to the angular separation, or its components, between the ILMT-observed and MPC-predicted positions exceeding one or more of the cited thresholds.